THE UNIVERSITY OF ADELAIDE

WEATHERING PRODUCTS AND GEOCHEMISTRY OF WASTE RESIDUES AT THE BRUKUNGA PYRITE MINE, ADELAIDE HILLS, S.A., IN RELATION TO ENVIRONMENTAL IMPACT.

by M. AGNEW. B.Sc.

November, 1994

Weathering products and geochemistry of waste residues at the Brukunga pyrite mine, Adelaide Hills, S.A., in relation to environmental impacts.

by

Mandy Agnew

11th Nov. 1994

Dept of Geology and Geophysics, University of Adelaide

This thesis is submitted as partial fulfilment of the Degree of Bachelor of Science (Honours) at the University of Adelaide.

National Grid Ref. (SI - 54), 6627 - I
(1 - 50,000)

TABLE OF CONTENTS

Table of Contents

List of Figure and Tables

Figures

Appendix C2

Tables

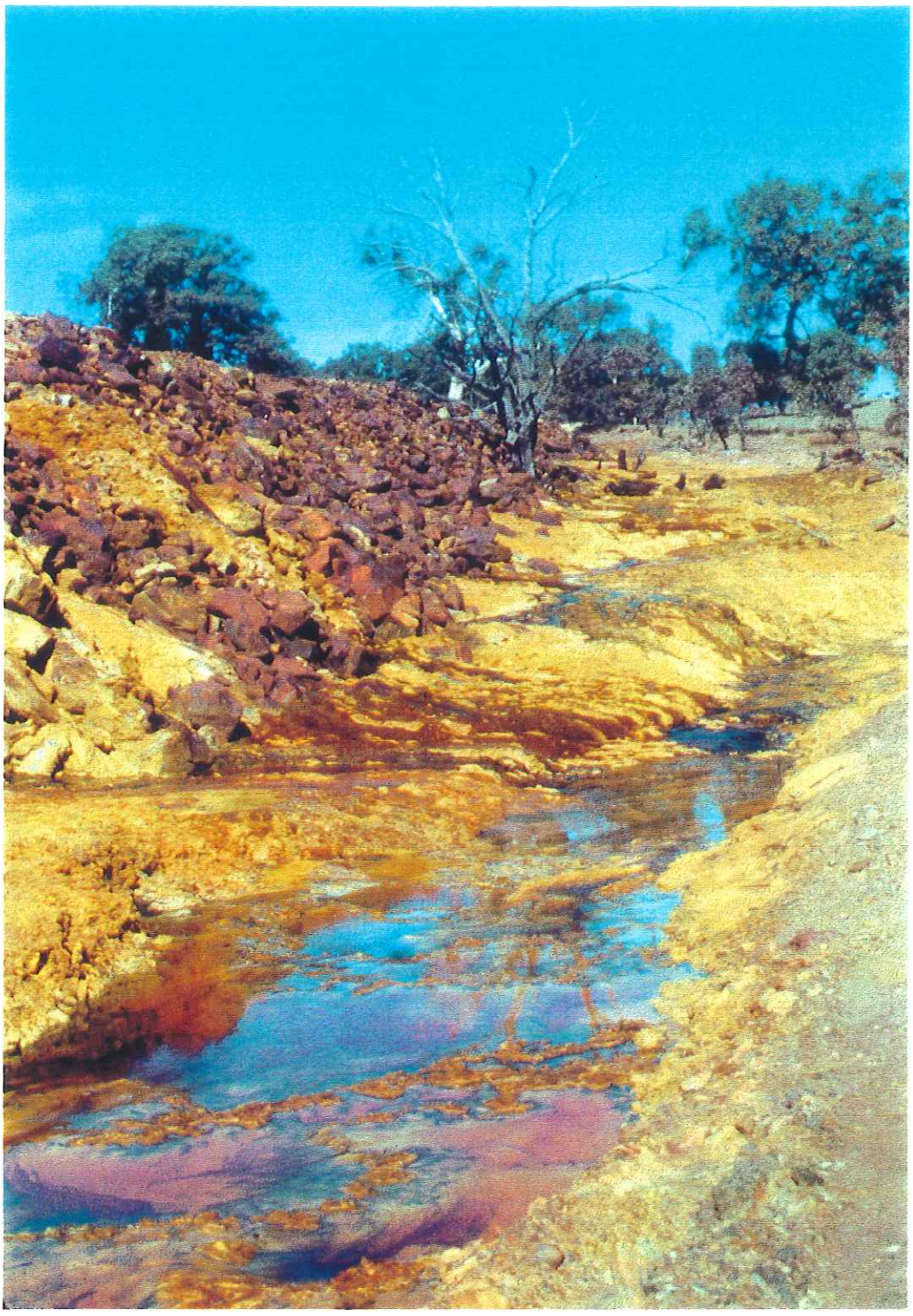

Acid Mine Drainage (AMD) developed at the Brukunga Pyrite Mine, South Australia.

ABSTRACT

The Brukunga Mine is located approximately 50 km east-south-east of Adelaide and was established in 1952 as a source of sulfur for superphosphate. Due to low sulfur prices, the mine was closed in 1972 and since that time has been a source of Acid Mine Drainage (AMD), which has in turn had a dramatic effect of the local and downstream environments.

Investigations into the waste dump and mine bench rocks indicate that large quantities of sulfides (up to 22%) are present. Oxidation of sulfides, catalysed by bacteria, quickly form a strongly acidic environment. The lack of significant quantities of rapid neutralising minerals, such as calcite, accentuates and enhances these low pH conditions. Resultant large quantities of acid and heavy metals produced through this oxidation are subsequently released into the surroundings. The contamination is enhanced by the release of lithophile elements formed during slow aluminosilicate neutralisation reactions that are taking place. The pollutants are released into Dawesley Creek, a tributary of the Bremer River, which flows through the mine site.

The tailings also add to the acidity problems through similar processes, but here sulfide quantities are much lower. A large accumulation of soluble salts has developed at depth and their location away from the zone of active oxidation indicates that oxidation has not been consistent through time. The development of a cemented layer region at 1-1.4m depth within the tailings is thought to be the preliminary stages of a hard pan. Calculations indicate that the formation of the cemented region is reducing the movement of the oxidation front and therefore the oxidation rate. Combining the two main observations suggests that the oxidation of the tailings is decreasing with time, through a self sealing action.

The current environmental hazard the tailings represents is significant. The groundwater movement through the tailings represents a major flushing effect, allowing water with high quantities of ferrous iron to be transported to the dam wall where it is readily oxidised.

This, combined with oxygen from the atmosphere causes the rapid oxidation of the rocks which make up the dam wall, and represents a major problem. A mechanism to reduce the ground water through-flow needs to be considered.

CHAPTER 1

INTRODUCTION

An understanding of physical and chemical characteristics of acid producing mine wastes is an environmental issue of fundamental importance. This project was initiated in order to increase our understanding of such processes through the study of Acid Mine Drainage (AMD) at the Brukunga mine.

The Brukunga Mine is located approximately 50 km east-south-east of Adelaide and 4 km north of Nairne (Fig 1.1). Between 1952 and 1972, the pyrite deposits were mined by Nairne Pyrites Ltd. to manufacture sulphuric acid for superphosphate production (SADME Conceptual plan April, 1989). Since abandonment, highly contaminated, acidic drainage from the mine has been polluting the local and down stream water and soil systems.

The aims of this study are to obtain an understanding of the physical and chemical characteristics of the mine and waste rocks, to determine the products of weathering and chemical reactions taking place within the tailings mass; and ultimately to investigate the potential for generation of Acid Mine Drainage (AMD). The position of each study locations is shown in Fig 1.2 which presents the lay out of the mine site.

Mining exposed the very large, dense and highly reactive sulfide formation to chemical attack. The sulfides present require oxygen and water to degrade, in turn producing sulfuric acid, mobile heavy metals and sulfate. Once started this process will not stop until all sulfide is converted to acid and iron sulphate, unless the access of oxygen can be prevented. The EWS (1993) reports that, the ore body has the potential to generate a total of 300, 000 tonnes of sulfuric acid.

Measures have been taken to minimise the effect on the environment via the implementation of a water treatment plant, seepage collection sumps and pump back systems during 1980-81 (Smith and Hancock, 1992). Additionally, covering and revegetation of the tailings dam and minor work on the waste dumps have been undertaken, along with experimental work on the quarry bench to determine the most appropriate sealing method.

A detailed review of the historical development of the mine, together with its geology, mining and processing is presented in Appendix A1. A general overview of rehabilitation procedures at the mine site is provided in Appendix A2, along with pollution associated with the hydrology of the area; the diversion techniques in use; the experiments taking

place on the mine bench and the neutralisation plant which plays an integral part in the rehabilitation strategy.

This thesis deals with field investigations carried out with two groups (ANSTO and Williams & Pannewig) who are currently working at the site. Analysis of the rocks at the site, including their chemical and mineralogical characteristics was undertaken for correlation with investigations into chemical and mineralogical changes occurring within the tailings dam. As a result of this, it is hoped constraints for minimisation of environmental impact may be determined.

This thesis, therefore summarises the current level of understanding of mine-site rehabilitation, in particular AMD generation and through the study of Brukunga mine enables future management of such sites to be carried out more effectively.

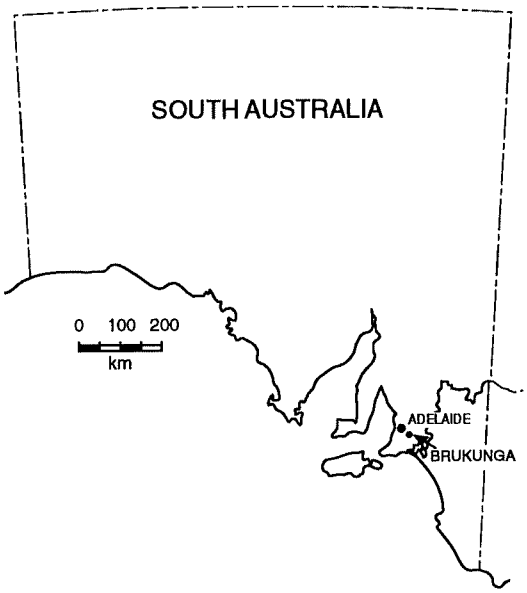

Fig 1.1: Locality map of The Brukunga Pyrite Mine

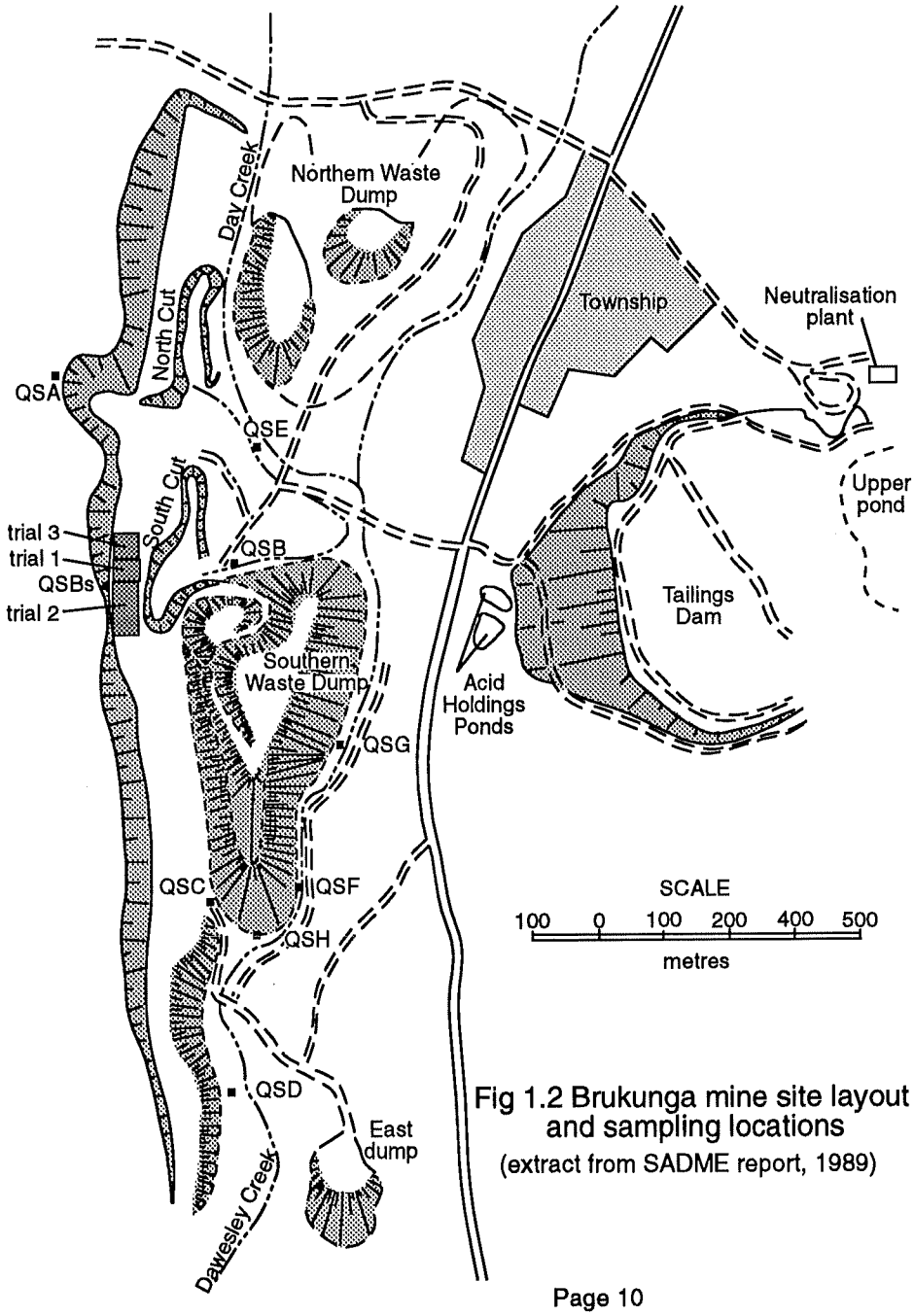

Fig 1.2 Brukunga mine site layout and sampling locations
(extract from SADME report, 1989)

CHAPTER 2

FIELD

INVESTIGATIONS

The Brukunga Pyrite Mine embodies the Talisker Calcsiltstone of the Kanmantoo Group, formally known as the Nairne Pyrite Member, found at the base of the Brukunga Formation.

The orebody is a conformable pyritic metasedimentary layer enclosed within regionally metamorphosed Kanmantoo Group rocks. Armstrong and Betheras (1952) described the ore body as being divided into five parallel bodies. The three major iron sulfide beds are approx. 15-30 m thick and the two waste beds are 5 m thick each. Ore zones consist of iron sulfide bearing-muscovite schists and gneisses with minor lenses of calc silicate and quartz plagioclase metasediments. The waste zones consist of quartz plagioclase granofels and minor calc silicate granofels, muscovite schists and gneisses. Thus, there is very little chemical difference in the silicate phase of ore and waste, the main difference being the iron sulphide content (Mason, G., 1968).

Problems perceived during site inspection included the weathering of sulfide rich waste rocks, and to a lesser extent deterioration of the mine bench . Groundwater seepage from the minesite and tailings dam containing high levels of dissolved metals and acid were also observed as discoloured water collected in seepage ponds at the base of the tailings wall. From this it was decided that field investigations at the minesite would consist of a collection of samples for detailed laboratory analysis from the mine bench, waste rock dumps and tailings dam. Investigations into the rock types present were undertaken to gain an appreciation of the processes taking place on the bench and in the waste rock dumps, which could then be applied to the tailings dam materials (see chapter 3).

Rock Sampling

Samples of each rock type were selected from the mine site as representative of the types and degree of weathering present. Investigation of these rocks provides detailed dissection of the mineralogy of the mine, the processes taking place, and their products. A review of observations and analysis is given in Chapter 3, section 3A, with detailed investigations recorded in Appendix C1.

Drillhole sampling

A network of groundwater and unsaturated zone gas sampling wells was installed in the tailings dam at the Brukunga mine by Australian Nuclear Science and Technology Organisation (ANSTO) in April 1994 as part of the rehabilitation program currently taking place. The unsaturated zone was drilled using a rotary auger rig and a percussion rig was used for below groundwater levels. During the drilling program, there was an opportunity to collect samples representative of each metre of each of the seven drill holes.

Undertaking this field investigation through preliminary sampling of the tailings dam allowed determination of the nature of the deposit, understanding of the depth and distribution of the water table in the dam and determination of the hydrology using an EM survey. An overall understanding of the tailings dam properties, then allowed appraisal for the position of a detailed core sampling site. Once the position was determined, samples were taken at 8cm intervals by hand auger in the vadose zone, and where possible in areas of special interest as intact cores inside stainless steel tubes. Intact cores in either stainless steel or PVC tubes were collected below the water table (see Appendix E for method). Results obtained through laboratory analysis of these samples is available in Chapter 3, section3B, with detailed observations accessible in Appendix C2.

Tailings Dam Preliminary Studies

Preliminary samples of tailings were obtained from every 1m depth of the tailings, at 7 different locations. The positioning of drill holes can be seen in Fig 2.1. Texture, colour, pH (in water and $CaCl_2$) and Electrical Conductivity (EC) were determined for each sample. Full details of the measurements are listed in Table 2B.1 of Appendix B. A material classification scheme was developed for the samples of tailings using the PATN software package see Appendix E for methods (Hollingsworth and Agnew, 1994).

Three groups of samples were identified by the first run of the classification (Table 2B.2 in Appendix B). Groups 1 & 2 together had only 10 members while group 3 comprised the remaining 122 samples. The important attributes for delineating groups are described in the box and whisker plots in Table 2B.3 Appendix B. They are as follows: Group 1 samples

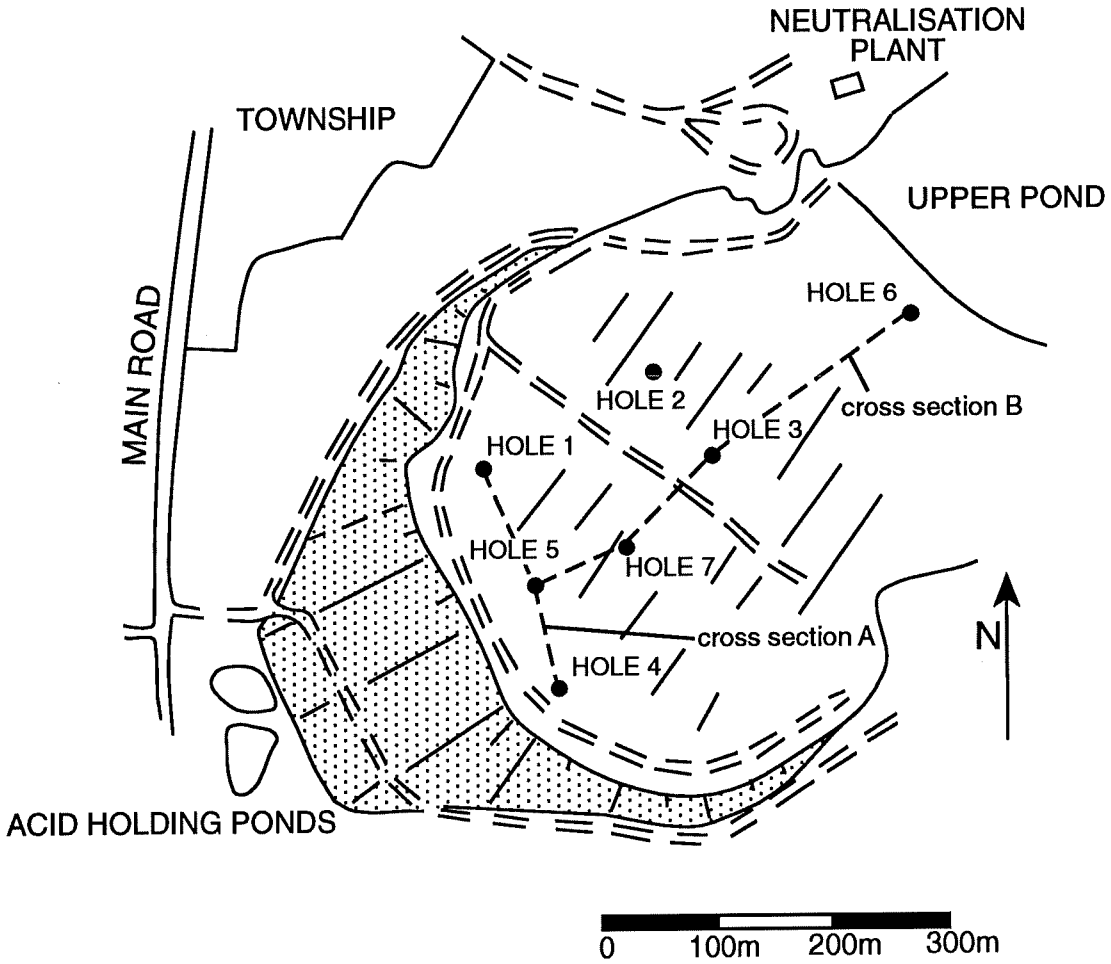

Fig 2.1: Brukunga Tailings Dam, indicating positions of bore holes and cross sections.

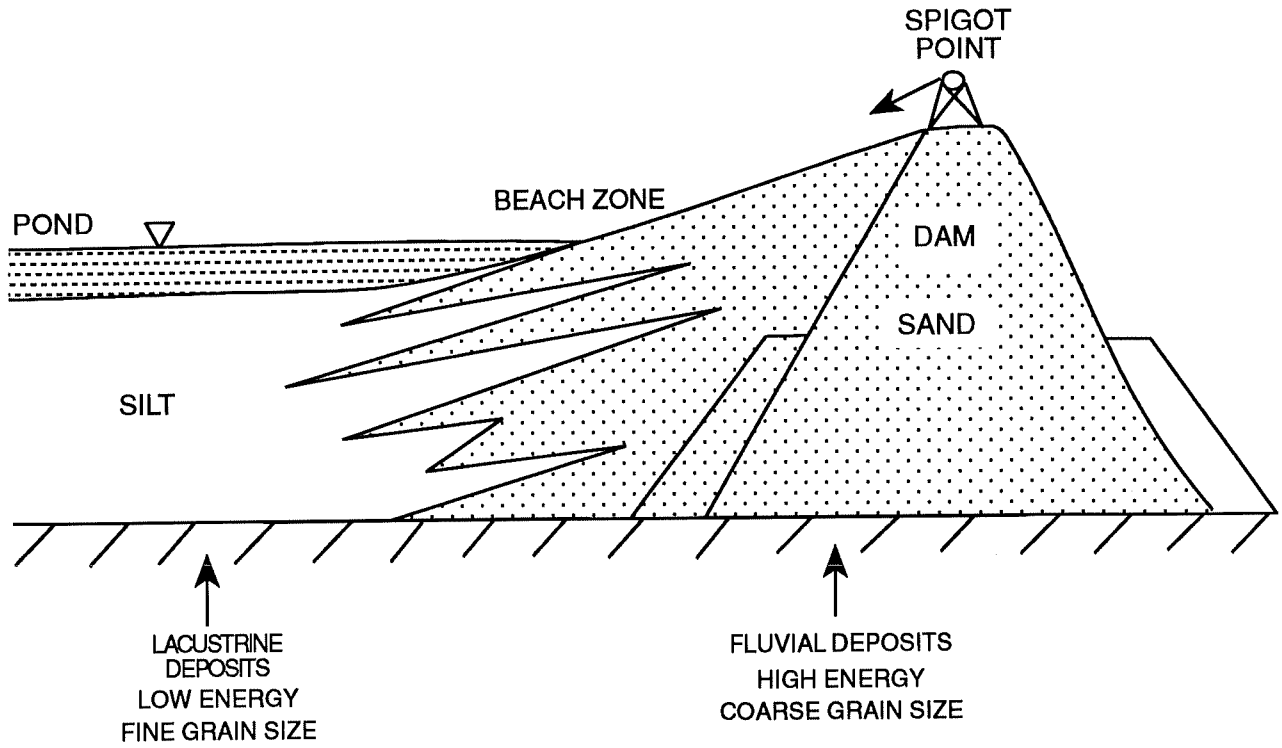

Fig 2.3 : A typical overview of the depositional environments of an impoundment receiving slurried tailings.

have high chroma (brown colour) and very low pH. The properties of this group arise from the oxidation of sulfidic tailings. Group 2 samples have neutral pH. These were sampled from the pre-existing land surface beneath the tailings dam and are samples of soil or bedrock which underlie the tailings. Group 3 comprises the majority of the samples. Generally these samples have low chroma (grey colour) and low to very low pH.

Group 3 samples were selected from the data set for further subdivision. Three further groups were produced (Table 2B.4 in Appendix B). From the box and whisker plots (Table 2B.5 in Appendix B) there is a clear distinction between subgroups on the basis of EC and pH values, with EC decreasing and pH increasing in going from subgroup 1 to subgroup 3. Subgroup 2 is coarser (sandy) than subgroup 3 (fine sandy-silt),while members of subgroup 2 tend to be deeper than other groups. A summary of these statistics is shown in Table 2B.6 in Appendix B.

The possibility of extended stratigraphic relations occurring within the dam was examined by preparing cross-sections along lines between drill holes. Cross-sections along holes 5, 7, 3 and 6 and again, at right angles to this, along holes 1, 5 and 4 are drawn in Figure 2.2a & b, with respect to sample classification and texture. The position of the water table is also shown as WT.

Correlations between holes were difficult to establish. The tailings exhibit a wide range of grain size variations, reflecting the different rates of deposition. Furthermore the slurry was discharged via spigotting points which were periodically moved.

The tailings deposits reflect two distinct depositional environments: a subaerial beach that extended outwards from the spigots, and a lacustrine zone that occurred where ponded water was present in the impoundment. A schematic view of the types of deposits in the tailings dam can be seen in Fig 2.3 (Jambor and Blowes, 1994).

During infilling of the tailings impoundment, the site of discharge points changed many times with the result that the relative position of the beach and pond also changed. Thus, at any one location there is likely to be substantial sedimentary heterogeneity observed in the profiles, as is demonstrably the case from the drillhole sections.

Two distinctly different sedimentary phases can be observed within the drillholes. Because of the fine grain size material of the slurry and the stabilisation problems this material had, the finest tailings were deposited in the centre of the dam (Bradshaw 1994). This was achieved by moving the spigots around the entire periphery of the dam allowing coarse material to build up at the edges to stabilize the system. Evidence of this comes from the predominantly fine material at the base of hole 3. As the mining operations continued and the stability of the dam wall was increased, a second depositional set up was undertaken.

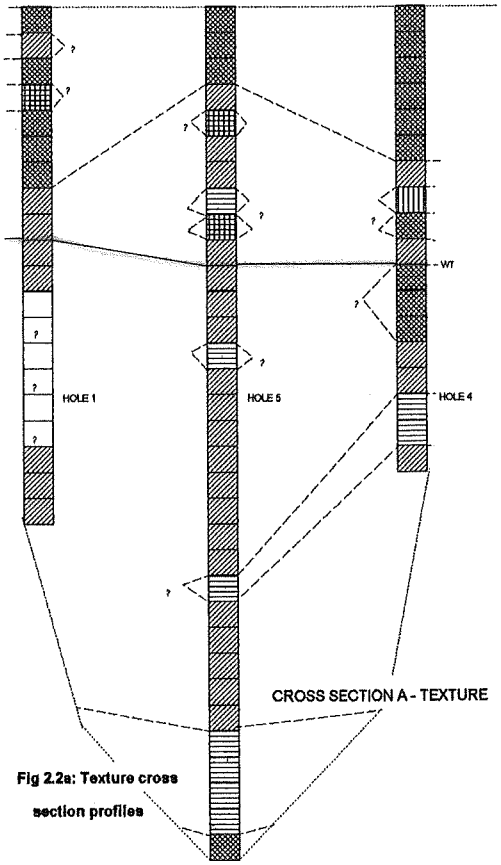

Fig 2.2a: Texture cross section profiles

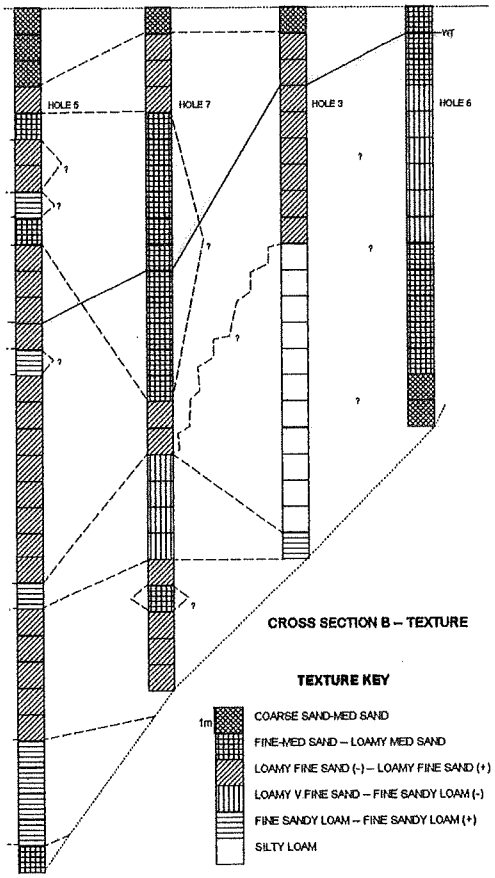

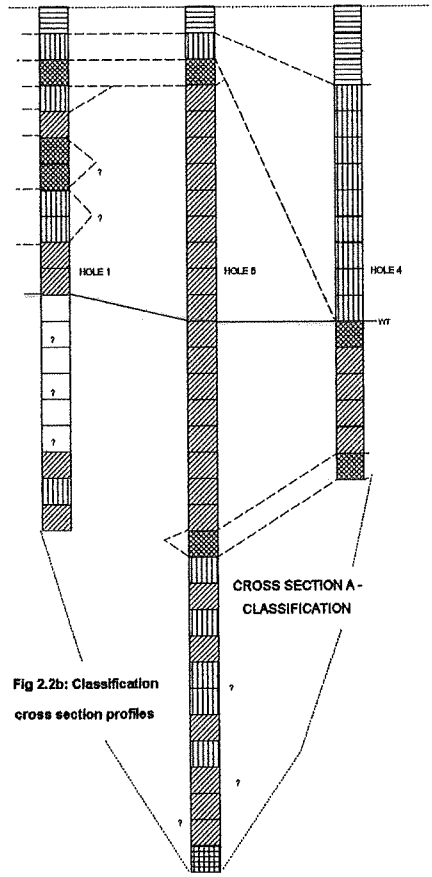

Fig 2.2b: Classification cross section profiles

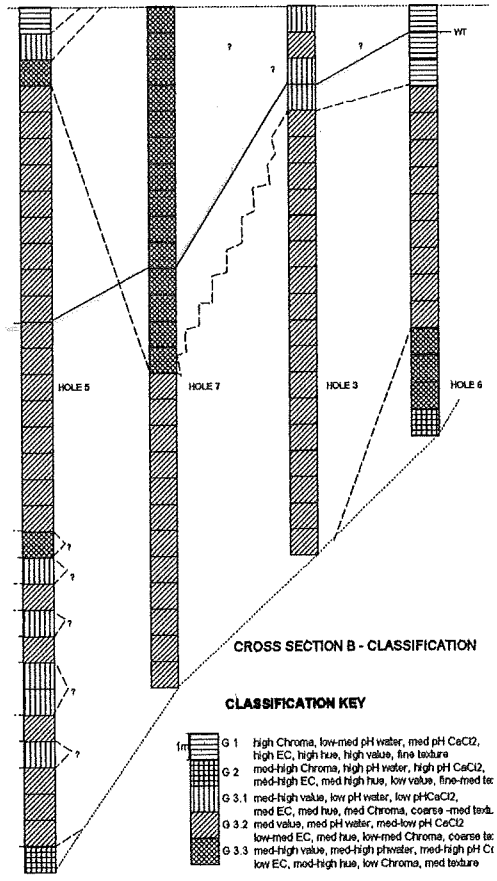

In this stage, a single pipe was extended out into the centre of the tailings dam and was broken at different lengths depending on the build up of material (Grindley 1994). Evidence of this stage comes from hole 3 where the fine material at the base terminates abruptly and is followed by a section of loamy fine sand and medium sand.

Correlations between drillhole profiles is difficult as distances between holes were in excess of 200m in some cases. Additionally the samples obtained were on average over 1m intervals with much of the fine sedimentary layering being obliterated. These fine layers were observed during detailed analyses of a core sampled profile (see chapter 3).

EC profiles measured in the tailings can be attributed to different types and quantities of salts that have precipitated at various levels. pH measurements reflect only minor changes in the tailings between pH 3-5, indicating that acid is generating in the vadose zone and leaching into the groundwater below. Generally the pH decreases with depth, as a result of concentration of the acid down the profile, and exhaustion of sulfide quantities and thus completion of acid formation at the surface.

Electromagnetic Survey

The results of the examinations of drillhole sample were combined with geophysical investigations to further understand the physical and geochemical nature of the tailings dam. During April 1994, a vertical EM survey was undertaken by Williams and Pannewig in the Brukunga tailings dam, using the methods discussed in Appendix E. Results of this survey can be seen in Fig 2.4. The objective of this was to determine whether a shallow sounding electromagnetic induction (EM) survey would be useful in:
a) detecting soluble salts resulting from the oxidation of sulfide tailings material, and
b) determining preferred flow paths (if any) within the tailings dam.

From the survey, apparent electrical conductivity (ECa) values ranged from 6 to 168 mS/m. The lowest values were associated with the rock outcrop in the S-E corner of the survey area whilst the highest occurred in the NE. In the west, ECa values were generally <30mS/m but there is some indication that plumes of higher conductivity material are fingering their way to the west.

High ECa values can be attributed to soluble salts which have formed in response to sulfide oxidation. In the presence of water the release of SO_4^{2-}, H^+ and Fe^{2+} and other metallic cations would occur, producing an electrically conductive material. Thus high ECa values are associated with soluble salts present in shallow groundwater.

Williams and Pannewig (1994), suggested that variations in ECa be attributed to differences in the clay and rock capping thickness or clay content of the capping. However little or no

Fig 2.4 Results of EM survey, with hole EC information and WT depth

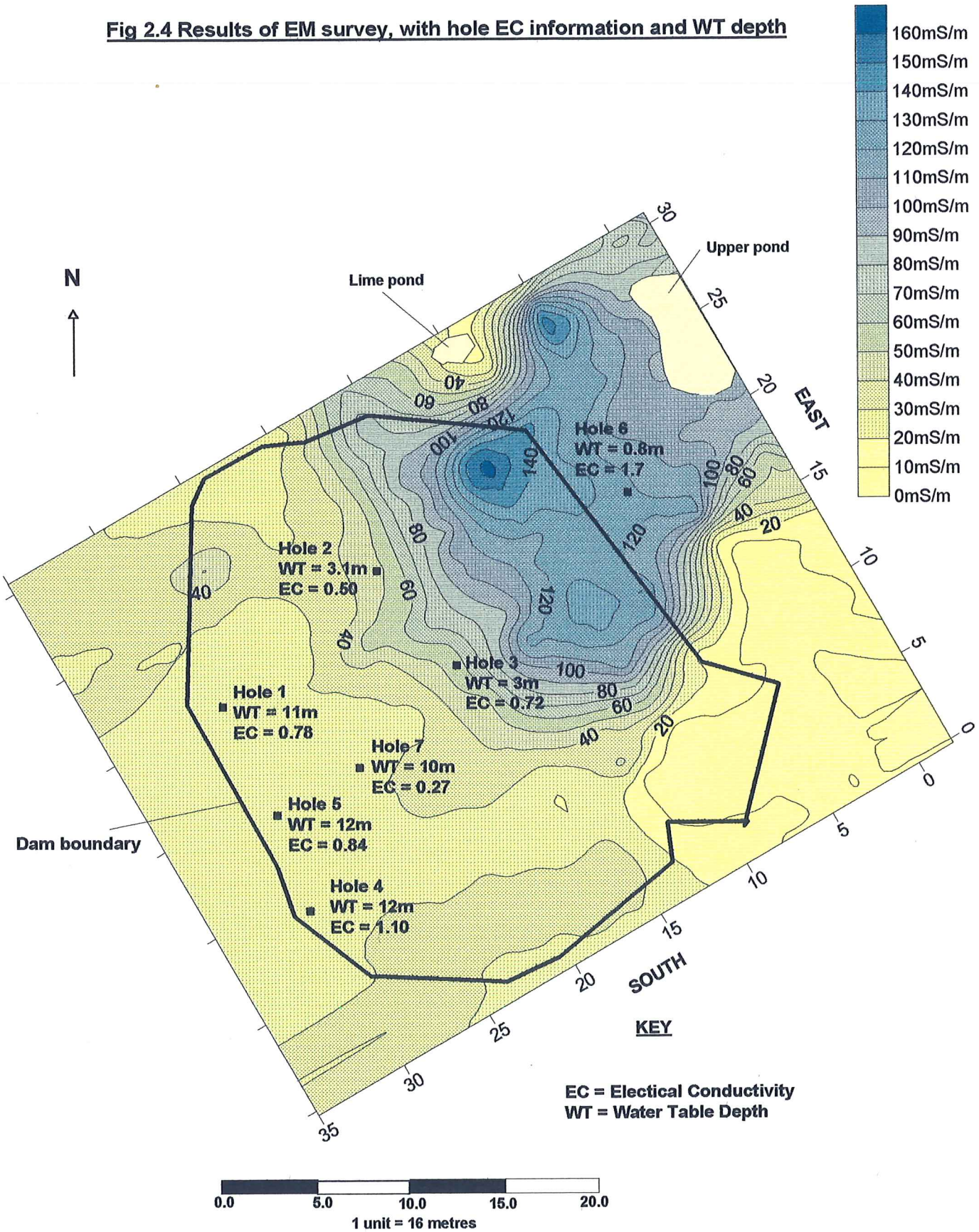

soil was used in the waste rock sewage sludge capping, and the cover that is present, is seldom thicker than 1m. Williams and Pannewig, (1994) also suggested that water table variations could be partly responsible for the data. However, they explained that it would be unusual for the groundwater body to have a cross section of this shape in a relatively uniform material unless some physical barrier existed within the profile.

The EM survey results combined with EC data collected from the 7 holes drilled during April 1994 may explain the results obtained. The effective depth of penetration of the signal from the EM31 instrument used by Williams and Pannewig in the survey in the vertical position, is generally taken to be about 5m (Williams and Pannewig 1994). The average EC values observed over the top 6m depth in the drillhole samples are shown in Fig 2.4 and are summarised below.

HOLE	Ave 6m EC (mS/m)	Approx ECa (mS/m)	Water Table Depth (m)
1	0.78	<30	11
2	0.50	50	3.1
3	0.72	55	3
4	1.10	<30	12
5	0.84	<30	12
6	1.70	125	0.6
7	0.24	<30	10

Apart from holes 6, 2 and 3 there seems little correlation between EC values and ECa values. At these sites the water table is between 0.8-3.1m depth, and thus is shallow enough to act as a conductor. Hole 6, has the highest EC and ECa recordings.

Holes 4, 5 and 1 show little correlation between EC and ECa. These drillholes have samples with some of the highest EC values and yet the lowest ECa results were obtained from these locations. The water table at these locations varies in depth from 11-12m.

The results obtained from the EM survey suggest a stronger correlation of ECa with water table depth rather than material EC. Preliminary studies of the dam indicated that the dam is far from homogeneous, and the water table in the area changes dramatically as a result of the heterogeneous nature of the material. It appears that the fine grained impervious nature of the tailings deposits that allows the water table to remain at shallow depths in some places, for example in the north east of the dam, while the coarse material to the west is quite pervious and allows through flow of water easily, thus lowering the water table. This EM survey also indicated the presence of fingers of deeper, higher conductive groundwater in the western part of the dam (Williams and Pannewig 1994).

The overview of the tailings dam assisted in the selection of a representative sample location required for detailed mineralogical identification and testing in the laboratory. A location adjacent to Hole 4 was decided upon for further sampling. This hole exhibited samples from four of the five groups over the shallowest depth.

CHAPTER 3

Laboratory studies of samples

Section 3A: Waste and mine rock laboratory investigations

Section 3B: Tailings laboratory investigations

Section 3A: Waste and mine rock laboratory investigations

Investigations of the rock samples allowed observations of the main ore and gangue minerals present in the mine and the subsequent degradation reactions occurring in response to AMD and the natural action of weathering. Examinations into the acid production and neutralisation potentials of the individual rocks give an indication of their potential environmental impact.

Classification of rock types through Net Neutralisation Potential

Laboratory analysis of waste and mine rock samples (for which the methods are detailed in Appendix E) are summarised in Table 3.1, with corresponding acid potential and acid consumption of each rock type and the overall Net Neutralisation Potential (NNP) ranking of each sample.

Table 3.1 Net Neutralising Potential of Rock Samples

Rock No.	S%	APP	AC	NNP	Ranking
1	7.9	241.7	8.7	-233	4
2	0.7	22.0	5.4	-17	11
3	2.8	85.7	6.3	-79	9
4	0.2	4.9	4.3	-1	12
5	24.5	749.7	1.7	-748	1
6	8.1	247.9	3.5	-244	3
7	3.6	110.2	2.3	-108	8
8	6.7	205.0	0	-205	6
9	5.6	171.4	0	-171	7
10	7.1	217.3	1.5	-216	5
11	15.1	462.1	1.4	-461	2
12	2.6	79.6	2.1	-77	10

A.P.P: Acid Producing potential kg H_2SO_4 per tonne
S%: Total percent sulfur
A.C: Acid Consumption/Neutralisation kg H_2SO_4 per tonne
N.N.P: Net Neutralising Potential (NNP = AC - APP)
Large values of APP indicates the rock type has a large potential to produce acid during interactions of oxygen and water with the sulfides present. Larger values of AC indicates the rock type has a larger potential for neutralising the acid formed during the oxidation of the sulfides. Neutralisation takes place through the alteration of minerals calcite and clinochlore and, less rapidly, with muscovite and biotite. The least negative result indicates that the sample has the greatest potential for neutralising the acid formed during oxidation of the sulfides. The lowest net neutralising potential is expressed as the most negative result, where the acid formation greatly outweighs the rocks neutralising capacity.
It should be noted that the ranking based on NNP, is the same as that obtained purely through total %S analysis. This indicates that the neutralising capacity of these rocks is low and has minimal effect on the overall outcome.

Characterisation of the rock samples into the most acid producing (least neutralising potential) to least acid producing (most neutralising potential) provides a basis for description of the acid producing and neutralising minerals present and their overall significance. Table 3.2 shows a summary of the rock samples present and their subsequent classification based on net neutralising potential.

The Net Neutralising Potential of the Brukunga waste rock samples ranges from (-750) to (-1) with an average of approximately 200 kg H_2SO_4 per tonne. Compared to values measured in mine sites around the world with AMD, for example waste rock from Currough and Heath Steel, Canada (Lawrence *et al*, 1989), it is comparatively high.

The H^+ generated by sulfide oxidation (see Table 3.3) in this mine dump is consumed by a series of mineral dissolution reactions. Acid neutralising processes are fundamental in controlling the environmental effects of wastes. In waste rock dumps and tailings dams alike, the balance between H^+ generating sulfide oxidation reactions and H^+ consuming mineral dissolution reactions controls the pH at the location of sulfide oxidation and at locations down gradient along the groundwater and surface water flow path. Buffering reactions that control the pH near the location of sulfide oxidation affect the rate of sulfide oxidation and the release of dissolved constituents into the groundwater. Investigations of each rock type were undertaken to identify their potential effects on the environment. It should be noted that neutralisation of AMD by mineral silicates is a relatively slow process and would not be captured in the assessment of acid consumption by the B.C Research Initial test. Thus the observed degradation of feldspars and micas noted in the samples has occurred in response to acid neutralisation over a long interval of time, and may represent pre-mining alteration.

Table 3.3 Sulfide Oxidation and Subsequent Precipitation Equations

pyrite oxidation

$$FeS_2 + 7/2O_2 + H_2O \Longrightarrow Fe^{2+} + 2SO_4^{2-} + 2H^+ \quad (3.1)$$

precipitation reaction

$$FeS_2 + 15/4O_2 + 7/2\ H_2O \Longrightarrow Fe(OH)_3 + 2SO_4^{2-} + 4H^+ \quad (3.2)$$

pyrrhotite oxidation

$$Fe(1-x)S + (2-x/2)O_2 + xH_2O \Longrightarrow (1-x)Fe^{2+} + SO_4^{2-} + 2xH^+ \quad (3.3)$$

chalcopyrite oxidation

$$CuFeS_2 + 4O_2 \Longrightarrow Fe^{2+} + 2SO_4^{2-} + Cu^{2+} \quad (3.4)$$

precipitation reaction

$$CuFeS_2 + 17/4O_2 + H_2O \Longrightarrow Fe(OH)_3 + Cu^{2+} + 2SO_4^{2-} + 2H^+ \quad (3.5)$$

Table 3.3 Cont Sulfide Oxidation and Subsequent Precipitation Equations

sphalerite oxidation

$ZnS + O_2 === Zn^{2+} + SO_4^{2-}$ (3.6)

where the Zn^{2+} cannot oxidise and ZnO_2 will only precipitate if it reaches an alkaline environment.

galena oxidation

$PbS + O_2 === Pb^{2+} + SO_4^{2-}$ (3.7)

precipitation reaction

$PbS + 5/2O_2\ H_2O === PbO_2 + SO_4^{2-} + 2H^+$ (3.8)

Note: in the case of equations 3.1, 3.2 and 3.3, precipitation of jarosite rather than ferrihydrite will occur if there is enough SO_4^{2-} already present, and this also releases almost as much H^+.

Hand Specimen, XRD and XRF Investigations

The minerals present in the rock samples were investigated by hand specimen observations, optical microscopy, SEM, XRD and XRF. Table 3.4 gives a summary of the XRF data obtained, while XRD results are summarised in Table 3.5. The minerals can be divided into primary and secondary constituents, with the primary minerals including ore and gangue components. Some of the minerals classified here as 'secondary' could have been formed from natural weathering processes due to acid conditions prior to mining. A list of these minerals is given Table 3.6.

Table 3.6 Minerals identified in rock samples

Primary minerals		Secondary minerals
Ore	Gangue	
pyrite FeS_2	anorthite $CaAl_2Si_2O_8$	jarosite $KFe_3(SO4)_2(OH)_6$
pyrrhotite $Fe(1-x)S$	albite $NaAl\ Si_3O_8$	alunite $KAl_3(SO_4)_2(OH)_6$
sphalerite ZnS	muscovite $KAl_3Si_3O_{10}\ (OH)_2$	kaolinite $Al_2Si_2O_5(OH)_4$
chalcopyrite $CuFeS_2$	quartz SiO_2	halloysite $Al_4Si_4O_{10}(OH)_8.8H_2O$
marcasite FeS_2	rutile TiO_2	sulfur S^o
galena PbS	zircon $ZrTiO_2$	hematite Fe_2O_3
	pyrophyllite $Al_4Si_8O_{20}(OH)_4$	rozenite $FeSO_4.4H_2O$
	clinochlore	kalinite $KAl(SO_4)_2.11H_2O$
	calcite $CaCO_3$	halotrichite $FeAl_2(SO_4)_4.22H_2O$
	tremolite $Ca_2Mg_5Si_8O_{22}(OH)_2$	gypsum $CaSO_4$
	anatase TiO_2	
	apatite $Ca_5(PO_4)_3(OH,F,Cl)$	
	biotite $K(Mg,Fe)_3(Si_3Al)O_{10}(OH,F)_2$	

Table 3.2 ROCK SAMPLE OVERVIEW

Rock Type	Rock No.	NNP	Degree of weathering	Comments
Group A : Very Low Net Neutralising Potential				
Highly weathered pyritic gneiss	5	-748	high	very large sulfide content strongest acid producer
Highly weathered metasediment	11	-461	high	large sulfide content sulfur produced on surface
Group B : Low Net Neutralising Potential				
Highly weathered coarse pyritic gneiss	6	-244	high	pyrite degradation forming hexagaonal voids
Massive pyritic quartzite	1	-233	mod	solid, impervious slow weathering
Fine grain pyrite-muscovite gneiss	10	-216	low-mod	impervious surface weathering only
Moderately weathered pyrite-muscovite gneiss	8	-205	mod	majority fine grained pyrite increased secondary minerals
Group C : Moderate Net Neutralising Potential				
Highly weathered pyritic gneiss	9	-171	high	highly reactive, rapid secondary mineral formation
Highly weathered fine grained pyritic metasediment	7	-180	high	well developed weathering profile formation of surface "skin"
Micaceous schist	3	-79	mod	low sulfide content, degradation to the elongate pyrite grains
Highly crystalline, highly weathered metasediment	12	-77	high	low sulfide content iron oxyhydroxide straining
Group D : Highest Net Neutralising Potential				
Tremolite rich metasediment	2	-17	low	unreactive, very low sulfide content , impervious
Highly weathered schist, originally pyritic	4	-1	high	no longer acid producing, sulfide degraded totally

(NNP units = kg CaCO3 equiv per tonne

Table 3.4 XRF DATA FOR ROCK SAMPLES

Rock Type	Rock No.	SiO2	TiO2	Al2O3	Fe2O3	MnO	MgO
Group A : V. Low Net Neutralising Potential							
Highly weathered pyritic gneiss	5	38.3	0.52	10.37	29.26	0.012	0.25
Highly weathered metasediment	11	43.6	0.5	10.91	21.51	0.049	1.56
Group B : Low Net Neutralising Potential							
Highly weathered coarse pyritic gneiss	6	55.8	0.59	14.53	11.22	0.045	1.74
Massive pyritic quartzite	1	54.3	0.61	13.35	14.35	0.151	2.48
Fine grain pyrite-muscovite gneiss	10	57.1	0.63	15.6	8.77	0.047	2.47
Moderately weathered pyrite-muscovite gneiss	8	66	0.73	11.81	8.23	0.008	0.41
Group C : Mod Net Neutralising Potential							
Highly weathered pyritic gneiss	9	71.6	0.8	7.17	7.49	0.01	0.27
Highly weathered fine grained pyritic metasediment	7	60.7	0.68	11.96	13.91	0.013	0.17
Micaceous schist	3	57.4	0.67	17.34	8.12	0.585	2.93
Highly crystalline, highly weathered metasediment	12	68.7	0.74	16.04	2.52	0.008	0.36
Group D : Highest Net Neutralising Potential							
Tremolite rich metasediment	2	52.2	1.48	14.58	9.75	0.284	6.6
Highly weathered schist, originally pyritic	4	64.9	0.81	16.74	6.04	0.032	1.22

	Rock No.	CaO	Na2O	K2O	P2O5	SO3	ZrO2
Group A	5	0.178	0.33	1.7	0.018	11.92	0.015
	11	1.43	1.2	3.02	0.046	21.49	0.014
Group B	6	1.57	1.7	3.38	0.059	14.22	0.013
	1	3.21	2.1	2.02	0.192	3.94	0.019
	10	1.87	1.9	3.27	0.096	8.2	0.015
	8	0.88	1.6	3.26	0.072	9.98	0.022
Group C	9	0.333	0.45	2.1	0.044	10.87	0.02
	7	0.291	0.46	2.49	0.041	5.98	0.019
	3	2.05	2	3.65	0.141	4.91	0.017
	12	1.92	3	3.65	0.051	4.59	0.016
Group D	2	9.68	1.7	1.28	0.183	1.71	0.014
	4	0.61	1	2	0.06	0.475	0.022

Table 3.5 SUMMARY OF XRD RESULTS FOR ROCK SAMPLES							
Rock Type	**Rock No.**	quartz	musco-	feldspar	pyrite	pyrrho-	clino-
			-vite			-tite	-chlore
Group A : V. Low Net Neutralising Potential							
Highly weathered pyritic gneiss	5	X	X	X	X		
Highly weathered metasediment	11	X	X	X	X		X
Group B : Low Net Neutralising Potential							
Highly weathered coarse pyritic gneiss	6	X	X	X	X		
Massive pyritic quartzite	1	X	X	X	X	X	X
Fine grain pyrite-muscovite gneiss	10	X	X	X	X		
Moderately weathered pyrite-muscovite gneiss	8	X	X	X	X		
Group C : Mod Net Neutralising Potential							
Highly weathered pyritic gneiss	9	X	X	X	X		
Highly weathered fine grained pyritic metasediment	7	X	X	X	X		
Micaceous schist	3	X	X	X			X
Highly crystalline, highly weathered metasediment	12	X	X	X	X		
Group D : Highest Net Neutralising Potential							
Tremolite rich metasediment	2	X		X	X	X	X
Highly weathered schist, originally pyritic	4	X	X	X			
	Rock No.	calcite	jarosite	rutile	tremolite	marcasite	sphal -
							-erite
Group A	5			X			
	11		X			X	
Group B	6		X				
	1	X	X	X			
	10		X			X	X
	8		X				
Group C	9		X			X	X
	7		X				
	3	X		X			
	12		X			X	
Group D	2	X			X	X	X
	4			X			
Rock Type	**Rock No.**	anatase	gypsum	pyro	kaolinite	rectorite	hematite
				-phyllite			
Group A : V. Low Net Neutralising Potential							
Highly weathered pyritic gneiss	5				X		
Highly weathered metasediment	11						
Group B : Low Net Neutralising Potential							
Highly weathered coarse pyritic gneiss	6		X				
Massive pyritic quartzite	1						X
Fine grain pyrite-muscovite gneiss	10						
Moderately weathered pyrite-muscovite gneiss	8						
Group C : Mod Net Neutralising Potential							
Highly weathered pyritic gneiss	9			X		X	X
Highly weathered fine grained pyritic metasediment	7						X
Micaceous schist	3				X		X
Highly crystalline, highly weathered metasediment	12						
Group D : Highest Net Neutralising Potential							
Tremolite rich metasediment	2	X					
Highly weathered schist, originally pyritic	4	X			X	X	X
	Rock No.	rozenite	halloy -	sulfur	alunite	halotrich-	kalinite
			- site			- ite	
Group A	5						
	11			X	X		
Group B	6		X			X	X
	1						
	10						
	8						
Group C	9	X		X			
	7						
	3						
	12						
Group D	2						
	4		X				

Review of SEM/EDX and Optical Microscopy for mine and waste rocks.

During weathering of the waste rocks, oxidation of the sulfides produces acid. The sulfides become degraded in different ways depending on their physical attributes. Observations of minor features of the degrading sulfides have been made using the scanning electron microscope with the associated microanalyser (SEM/EDX), and thin section optical microscopy. The EDX spectra that accompany SEM and thin section photographs are referred to as subscripts of the main photographs (eg SEM photograph is referred to as Fig 3.11 and accompanying EDX spectra is Fig 3.11a). A complete summary of the EDX spectra may be found in Appendix C1.

The largest quantity of sulfur, predominantly as sulfide, occurs in rock 5, a highly weathered pyritic schist. Under the SEM/EDX, the pyrite crystals present showed conchoidal fracturing which produced subhedral forms in varying states of degradation. Crystals ranged from only slightly weathered to moderately weathered, in which dissolution produced depressions (Fig 3.1).

Dissolution of crystals also occurred in *Rock 6*, a highly weathered coarse pyritic gneiss. Here, high resolution observations of crystals showed strongly pitted surfaces with hexagonal shaped voids (Fig 3.2). The voids may represent the removal of less resistant iron sulfide, (eg. pyrrhotite) from these sites. In some places small spherical jarosite accumulations are observable.

Similarly in *Rock 1*, a massive pyritic quartzite, individual pyrite faces could be seen to be decaying along planes of low resistance to prevailing weathering conditions (oxygen and water access). This weathering has resulted in a finger-like structure with the more resistant material existing long after the weaker sections have been removed (Fig 3.3 & 3.4).

The main weathering product of *Rock 5*, a highly weathered pyritic schist, appears to be kaolinite ($Al_4\ Si_4O_{10}(OH)_8$). SEM/EDX also identified halloysite ($Al_4Si_4O_{10}(OH)_8.8H_2O$) a hydrated form of kaolinite, on both the pyrite and other minerals (Fig 3.5 & 3.5a). Kaolinite can be formed principally via the weathering of feldspars, feldspathoids and other silicates, eg muscovite and pyrophyllite, possibly as:

$$2NaAl\ Si_3O_8 + H^+ + 9/2H_2O \equiv\equiv 1/2Al_2Si_2O_5(OH)_4 + Na^+ + 2Si(OH)_4 \qquad (3.9)$$

albite kaolinite

$$CaAl_2Si_2O_8 + 2H^+ + H_2O \equiv\equiv Ca^{2+} + Al_2Si_2O_5(OH)_4 \qquad (3.10)$$

anorthite kaolinite

$$KAlSi_3O_8 + H^+ + 9/2H_2O \longrightarrow K^+ + 2H_4SiO_4 + 1/2Al_2Si_2O_5(OH)_4 \quad (3.11)$$

k-feldspar kaolinite

$$Al_4Si_8O_{20}(OH)_4 + 10H_2O \longrightarrow 2Al_2Si_2O_5(OH)_4 + 4Si(OH)_2 \quad (3.12)$$

pyrophyllite kaolinite

Kaolinite can be formed under normal weathering conditions. However, the system is probably accelerated due to the presence of H^+ ions. The H^+ ions are supplied through the oxidation of FeS_2. Halloysite forming in response to feldspar, mica and pyrophyllite weathering can be observed in Fig 3.6 where it coats the particles. The main alteration products observed in thin section occur in the fine matrix of the rock, particularly along contact boundaries with pyrite crystals (Fig 3.7 (frame width 0.5mm), 3.7a, 3.7b & 3.7c). The altered pyrite crystals and gangue minerals show orange staining which can be attributed to the presence of iron oxides. In locations where muscovite is in direct contact with the pyrite crystal, reaction rims are present, in which muscovite is altering to kaolinite (Fig 3.8 (frame width 0.5mm)).

A different weathering path is shown in *Rock 11*, highly weathered metasediment, has only oxidised as far as elemental sulfur which formed amorphous agglomerations (Fig 3.9,3.9a & 3.10). The possible reaction is:

$$FeS_2 + O_2 + 4H^+ \longrightarrow 2Fe^{2+} + 4S^o + 2H_2O \quad (3.13)$$

pyrite sulfur

In thin section, sulfur formation is clearly associated with the degradation of pyrite, and the sulfur occupies the voids left where pyrite crystals once existed, along with minor jarosite (Fig 3.11 (frame width 0.5mm) & 3.11a). Nordstrom (1982) explains the formation as a loss of ferrous ions from lattice sites of pyrite, leaching an unstable sulfur-rich surface which eventually disrupts and reorganises into elemental sulfur. Because sulfur is so readily utilized by bacteria, it is unusual to find it in elemental form.

Both jarosite ($KFe_3(SO4)_2(OH)_6$) and alunite ($KAl_3(SO_4)_2(OH)_6$) are present in this rock. Jarosite occurs mainly as a coating to all minerals present except sulfur (Fig 3.12). Initially pyrite is oxidised sending Fe^{2+} into solution (eq 3.1) which is itself subsequently oxidised by oxygen to produce Fe^{3+}. *T. ferrioxidans* are iron-oxidizing bacteria which act as catalysts in this reaction. They are reported to speed up the reaction by approximately one million times (Stumm and Singer 1970). The role of bacteria is discussed in detail in Appendix D.

$$4Fe^{2+} + O_2 + 4H^+ \xrightarrow{T.ferrioxidans} 4Fe^{3+} + 2H_2O \quad (3.14)$$

Jarosite may then be precipitated out of solution

$$K^+ + 3Fe^{3+} + 2SO_4^{2-} + 6H_2O \text{ === } \underset{\text{jarosite}}{KFe_3(SO_4)_2(OH)_6} + 6H^+ \quad (3.15)$$

where K^+ is present in solution due, for example to the weathering of muscovite

$$2\underset{\text{muscovite}}{KAl_3Si_3O_{10}(OH)_2} + 3H_2O + 2H^+ \text{ === } 3\underset{\text{kaolinite}}{Al_2Si_2O_5(OH)_4} + 2K^+ \quad (3.16)$$

Alunite precipitates through a similar process, where Al^{3+} is derived from the decomposition of aluminosilicate minerals.

$$K^+ + 3Al^{3+} + 2SO_4^{2-} + 6H_2O \text{ === } \underset{\text{alunite}}{KAl_3(SO_4)_2(OH)_6} + 6H^+ \quad (3.17)$$

In sample *Rock 6*, a highly weathered coarse pyritic gneiss, hematite (Fe_2O_3) has formed instead of jarosite, presumably because sulfate concentrations were decreased by leaching.

$$Fe^{3+} + 3H_2O \text{ === } Fe(OH)_3 + 3H^+ \quad (3.18)$$

$$2Fe(OH)_3 \xrightarrow{\text{dehydration}} Fe_2O_3 + 3H_2O \quad (3.19)$$

During a period when the rock was water saturated and then allowed to dry out, pale yellow fibrous crystals developed. XRD analysis indicated these were a mixture of kalinite ($KAl(SO_4)_2.11H_2O$) a fibrous type of K-Al alum, halloysite and halotrichite ($FeAl_2(SO_4)_4.22H_2O$) and gypsum. The fact that these minerals are not observed on this rock in the field may be due to its exposed positioning, from which these soluble minerals are readily leached.

Coatings of rozenite and jarosite have formed on the surface of *Rock 8*, a moderately weathered pyrite-muscovite gneiss. Additionally, minor sulfur was observed developing in depressions. The jarosite exists as pale yellow rhombohedrals and has precipitated from solution (eq 3.15). Rozenite, identified through XRD, appears as a white powder, also precipitates from solution as the rock dries out.

$$Fe^{2+} + 4H_2O + SO_4^{2-} \text{ === } \underset{\text{rozenite}}{FeSO_4.4H_2O} \quad (3.20)$$

A highly acidic environment is indicated in *Rock 9*, a highly weathered pyritic gneiss. Within this sample minerals have been totally degraded to skeleton remains, and secondary

minerals have developed unusual forms in response to rapid precipitation from solution. Many different secondary mineral phases were observed, (Fig 3.13 & 3.14) including fibrous halotrichite (Fig 3.15, 3.15a & 3.16), stringers of opal A (Fig 3.17 & 3.18) and barytes ($BaSO_4$). A platy-fibrous material was also observed and subsequently shown by EDX analysis to be an iron sulfate, most probably rozenite, as this mineral was identified by XRD (Fig 3.19 & 3.19a). Elemental sulfur and hematite were also identified. The fibrous nature of rozenite and halotrichite suggest that they precipitated quickly from solution, halotrichite forms in a similar manner to rozenite (eq 3.20) as:

$$Fe^{2+} + 2Al^{3+} + 4SO_4^{2-} + 22H_2O \rightleftharpoons \underset{\text{halotrichite}}{FeAl_2(SO_4)_4.22H_2O} \qquad (3.21)$$

The occurrence of opal A as stringers (Fig 3.17 & 3.18) suggests it developed as a residue after the dissolution of a pre-existing mineral phase. Evidence of this comes from opal observed in the shape of mica (Fig 3.20), where all other constituents of the mica have been leached out leaving only the framework of silica. Additional opal A was observed with little or no structure. This may have formed though direct precipitation from a silica-rich solution.

Within *Rock 7*, a highly weathered fine grained pyritic metasediment, a well developed weathering skin exists. At the surface, the secondary products jarosite and goethite are abundant, while pyrite and albite are non-existent. Approximately 1cm below the surface pyrite crystals are apparent. They are very fine grained, and all crystals detected showed pitting to some extent. Within 3mm of the surface, albite can be observed. Boxwork structures are observed where pyrite has been degraded.

Thin section studies showed kaolinite in reaction rims between neighbouring muscovite and pyrite (Fig 3.21 (frame width 0.5mm)), and generally distributed throughout the rock matrix as a coating to quartz and muscovite alike. Hematite is also a minor weathering product of this rock forming red spheres and minor staining along regions where pyrite has been totally degraded (Fig 3.22 (frame width 0.5mm) & 3.22a).

Rock 3, micaceous schist, again clearly demonstrates the degradation of gangue minerals as a whole and the development of widespread secondary minerals, in this case goethite, throughout the matrix. Fig 3.23 (frame width 0.5mm) shows the alteration of muscovite along cleavages and grain boundaries, leaving them stained with goethite.

The fine texture of the tremolite-rich metasediment *(Rock 2)* has resulted in a low level of sulfide degradation and thus decreased secondary mineral formation. Optical microscopy showed pyrite present in small quantities and that weathering is restricted to the surface or

along fractures within the rock. The main products of weathering are jarosite and iron oxy-hydroxides that form a conspicuous coating along fractures and on the rock surface.

An originally pyritic highly weathered schist *(Rock 4)* exhibited the most advanced state of weathering observed within this suite of rock samples. The sulfur concentration measured in this rock is 0.7% (Table 3.1) but no sulfides were observed microscopically, and the S probably represents minor amounts of sulfate. In thin section there are extensive red-orange stains associated with voids where pyrite formerly existed (Fig 3.24 (frame width 0.5mm)). SEM/EDX investigations identified the stains as iron oxyhydroxides, including localised hematite spheres and minor jarosite (which could account for the sulfur). This iron staining was usually confined to fractures in mica which have been zones where dissolved iron moved through the rock. Leaching would also account for the absence of any major amounts of sulfates and other weathering products.

Potential Environmental Impact

The rock types described were selected as representative of the range of materials in the waste rock dump and mine bench from which AMD could develop through sulfide (pyrite) degradation. Each rock type because of its particular composition and structure, represents a different potential impact on the local environment of the mine site and possibly the wider environment, depending on its abundance. Examples of this follow:

Rock 5 - highly weathered pyritic schist

If the highly weathered pyritic schist (*rock 5*) was a major component of the mine and waste rock dumps, then this rock would have a major detrimental effect on the surrounding environment. It is the sheer quantity of pyrite present within this specimen that produces the highest ranking AMD potential (NNP = -748, Table 3.1). The muscovite present has some neutralising capacity (Jambor and Blowes, 1994), but this is insignificant compared to the quantity of sulfide available. Thus leaching of this rock would cause large quantities of acid and metallic elements to enter the water system.

Rock 11 - highly weathered metasediment

Rock 11 would similarly effect the environment due to the large quantity of pyrite present. Additional acidity would result from the chalcopyrite and sulfur also present. The reactions of chalcopyrite ($FeCuS_2$) were previously given in equations 3.4 and 3.5. Subsequent oxidation of sulfur again creates more acidity.

$$2S^{o} + 3O_2 + 2H_2O \longrightarrow 2SO_4^{2-} + 4H^{+} \qquad (3.22)$$

sulfur

Jarosite present in the rocks produces acidity during the initial flush of AMD (eq 3.15), but it can play a further role after most of the pyrite has oxidised. If the system is then leached with rain so that soluble SO_4 is removed, it changes slowly to $Fe(OH)_3$ and releases more acid

$$\underset{\text{jarosite}}{KFe_3(SO_4)_2(OH)_6} + 3H_2O \Longrightarrow 3Fe(OH)_3 + K^+ + 2SO_4^{2-} + 3H^+ \qquad (3.23)$$

On the other hand, if there is any residual acid about (perhaps retained on the mineral surfaces), then it could have a neutralising effect by reaction of H^+ with its hydroxyl groups (Jambor and Blowes, 1994). However, this effect might only be temporary, since Fe^{3+} bought into solution could later be reprecipitated as $Fe(OH)_3$ and again add acid. Thus the effect of jarosite on the system is finely balanced to external conditions.

The combination of the fine grained nature of this sample; the sulfur and sulfides present, and the lack of major neutralising minerals means that this rock type still has a large potential for producing an environmental hazard to surrounding terrain.

Rock 6 - highly weathered coarse pyritic gneiss

Due to the relatively moderate amount of pyrite present, the NNP of R*ock 6* was -244. This is quite substantial compared to many samples. The potential neutralising minerals present are muscovite (eq 3.16) and biotite which reacts according to:

$$\underset{\text{biotite}}{K(Mg,Fe)_3(Si_3Al)O_{10}(OH,F)_2} + 4Al^{3+} + 3H_2O + 2H^+ \Longrightarrow \underset{\text{kaolinite}}{3Al_2Si_2O_5(OH)_4} + 2K^+ + 3Fe^{2+} + 3Mg^{2+} \qquad (3.24)$$

The micas are obviously reacting to some extent, as shown by their degraded nature (Fig 3.25). Cleavages are spreading with alteration minerals precipitating between layers.

Rock 1 - massive pyritic quartzite

The potential effect of *rock 1* on the environment is distinctly different because of the presence of the neutralising minerals, calcite and clinochlore. Calcite is highly neutralising, but it would have no significant effect here due to the small quantity present:

$$2H^+ + \underset{\text{calcite}}{CaCO_3} \Longrightarrow Ca^{2+} + H_2CO_3 \qquad (3.25)$$

The specimen also contains 5-10% clinochlore. This aluminosilicate has a strong neutralising capacity because of its brucite-like $(MgAl)_6(OH)_{12}$ interlayers, and the dissolution of this mineral would have a significant effect on the AMD potential (Fordham,

1994). The products of weathering must have leached out of the system as only minor kaolinite was observed and Mg and Al weathering products were absent.

During SEM/EDX investigations, the clinochlore within this specimen did not appear to be weathering differently from the muscovite present. Muscovite alteration was clearly evident in thin section, and biotite was also seen to degrade into a K leached end member aluminosilicate (Fig 3.26 (frame width 0.5mm) 3.26a & 3.26b). However the combination of all three minerals proves to be ineffective during the short term, as shown by the NNP of -233.

Rock 7 - highly weathered fine grained pyritic metasediment

The NNP of *rock 7* was comparatively low (-108) compared to the other rocks investigated. This can be attributed largely to the low total sulfur content 3.6%. The neutralising capacity of the muscovite would have some effect.

Rock 2 -tremolite-rich metasediment

This rock had the second least negative NNP (-17) of all the rocks observed due to the low quantity of sulfides present. Some of the AMD produced would be neutralised through the dissolution of biotite (eq 3.24), calcite (eq 3.25) and clinochlore. However, as explained before, the fine grained impervious nature of this rock prevents much reaction taking place. Thus the effect on the environment is low, as a consequence of the physical and chemical properties of the rock.

Rock 4 - highly weathered schist- originally pyritic

Rock 4, had the least negative NNP (-1) of all the samples investigated, because of the very low total S%. Thin section analysis showed extensive iron staining associated with pyritic voids. This sample, originally pyritic, no longer has the potential to have any major effect on the surrounding environment. Additionally the micas present would reduce any further AMD produced. It should be noted that unweathered counterpart of this rock type, would still represent a substantial hazard to the surroundings.

These examples clearly illustrate that the environmental impact is a consequence of factors such as the physical morphology of the rock, the amount and type of sulfides and neutralising minerals present, the presence of protective coatings on grains by secondary minerals, and the location of the rock within the mine dump, ie. in exposed and leached or in sheltered positions.

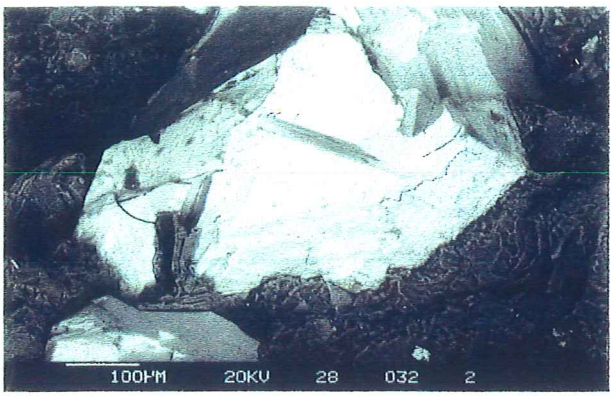

Fig 3.1 Pyrite dissolution - rock 5.

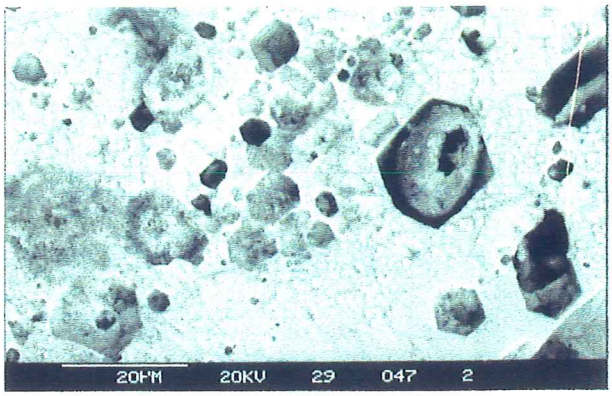

Fig 3.2 Hexagonal voids developed on pyrite crystal face - rock 6

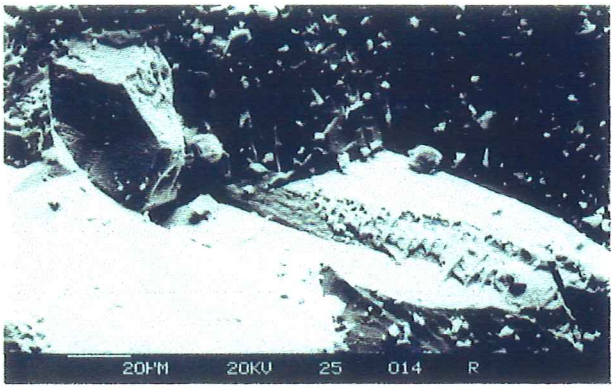

Fig 3.3 Alteration of pyrite crystal face - rock 1.

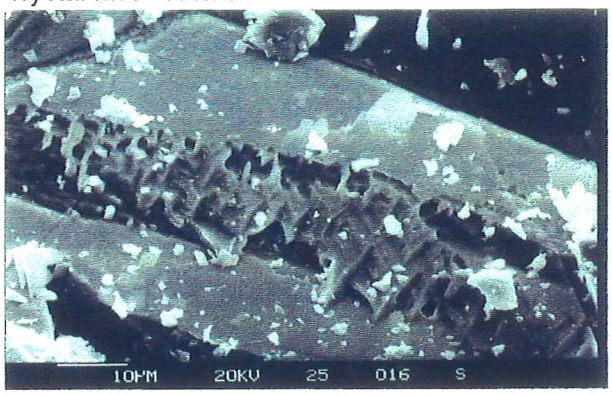

Fig 3.4 Close up of alteration along pyrite crystal face - rock 1.

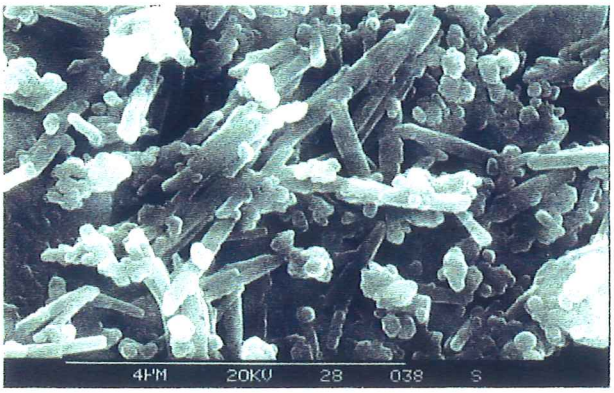

Fig 3.5 Close up of halloysite on pyrite crystal - rock 5

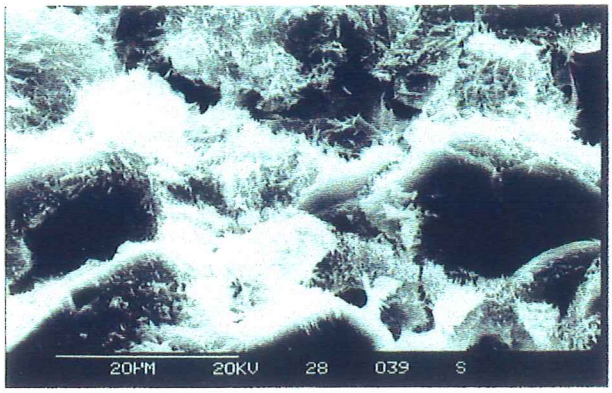

Fig 3.6 Halloysite coating of host crystals - rock 5

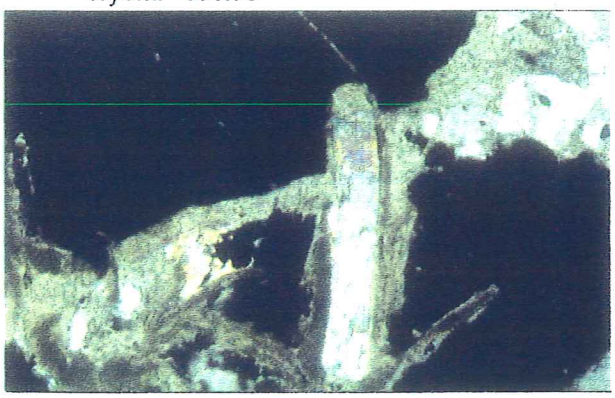

Fig 3.7 Kaolinite reaction rim developed between pyrite and muscovite - rock 5.

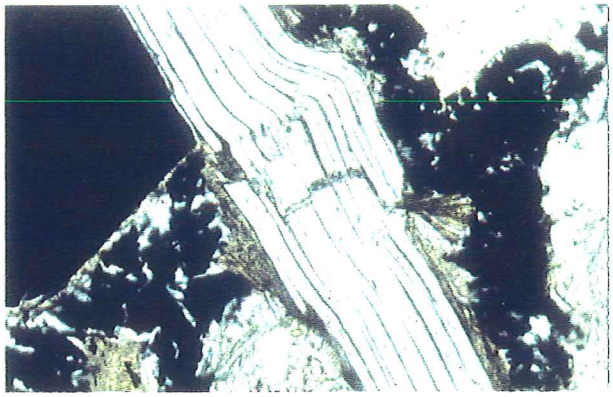

Fig 3.8 Iron staining and kaolinite developed from muscovite degradation - rock 5.

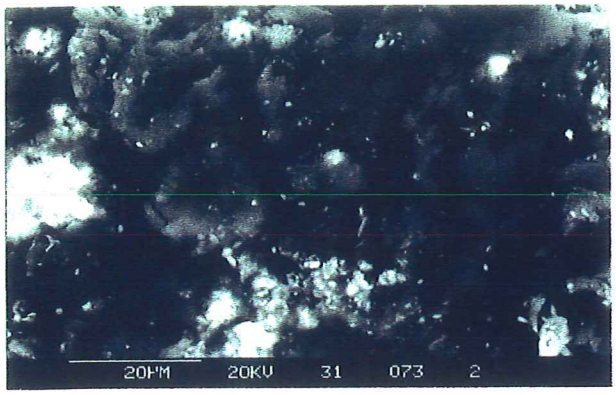

Fig 3.9 Amorphous sulfur accumulations - rock 11.

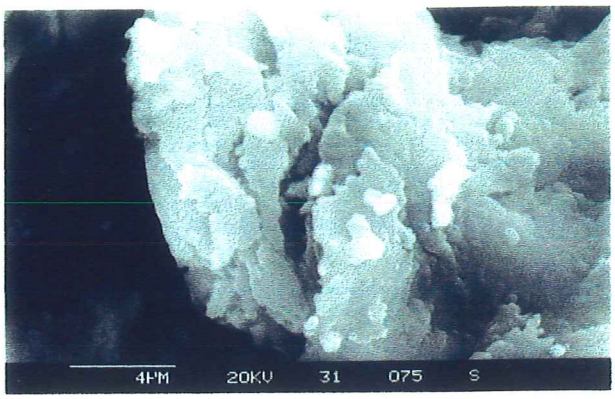

Fig 3.10 Close up of sulfur accumulations - rock 11.

Fig 3.11 Sulfur formation within voids of pyrite degradation - rock 11.

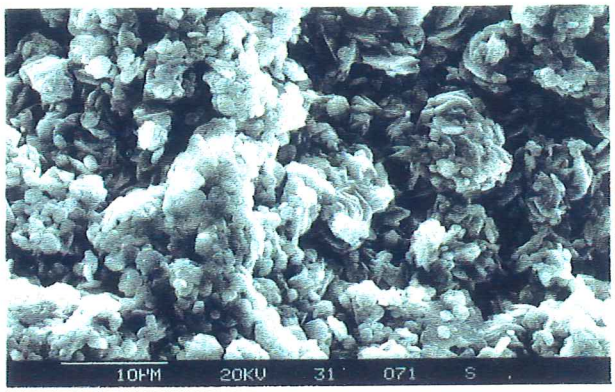

Fig 3.12 Jarosite coating developed on host - rock 11.

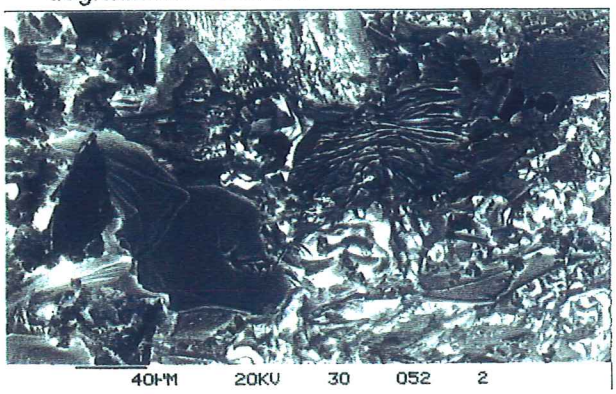

Fig 3.13 Overview of secondary mineral assemblage - rock 9.

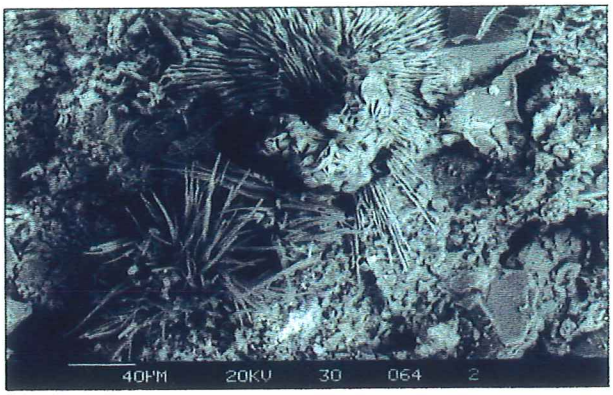

Fig 3.14 Overview of secondary mineral assemblage - rock 9.

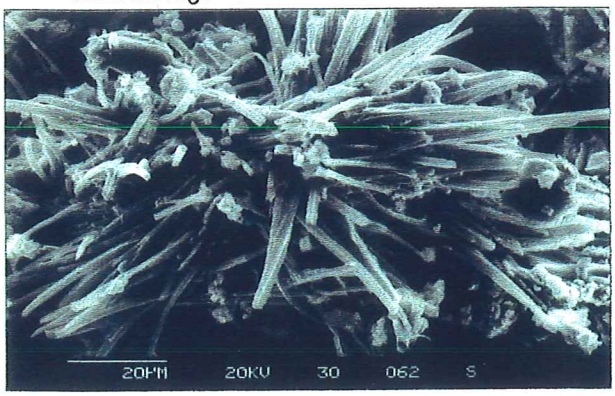

Fig 3.15 Fibrous halotrichite - rock 9.

Fig 3.16 Close up of halotrichite - rock 9.

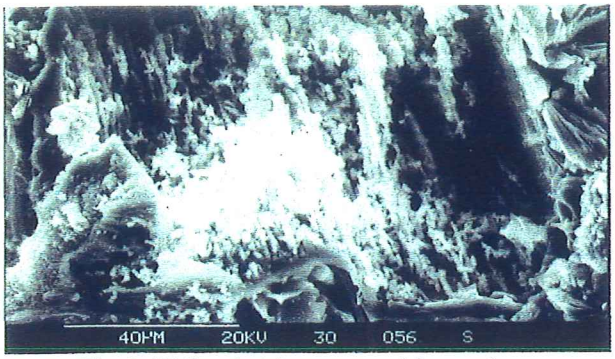

Fig 3.17 Opal stringers, residues of aluminosilicate degradation - rock 9.

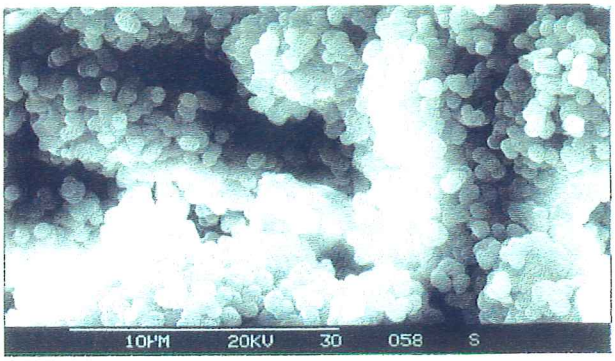

Fig 3.18 Close up of opal - rock 9.

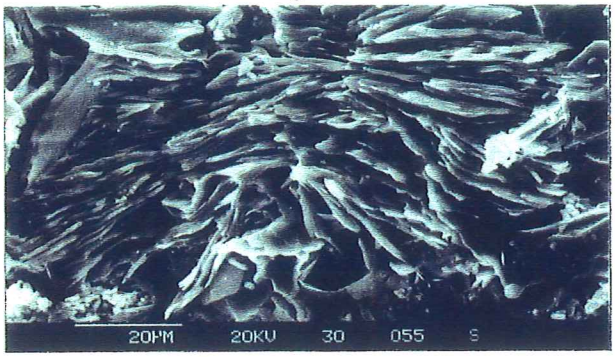

Fig 3.19 Platy fibrous iron sulfate, probably rozenite - rock 9.

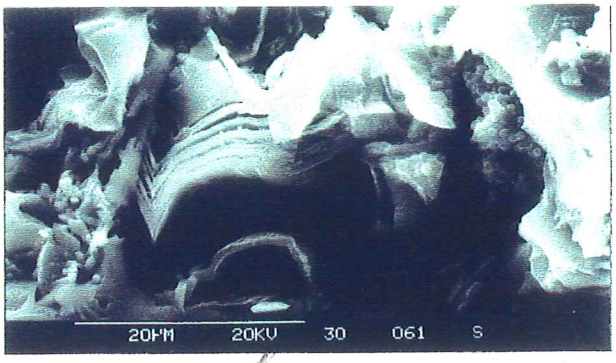

Fig 3.20 Remanaent mica structure, formed only by silica - rock 9.

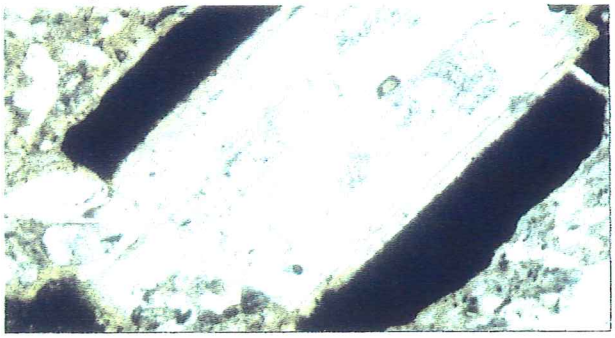

Fig 3.21 Reaction rims of kaolinite developed between pyrite and muscovite - rock 7.

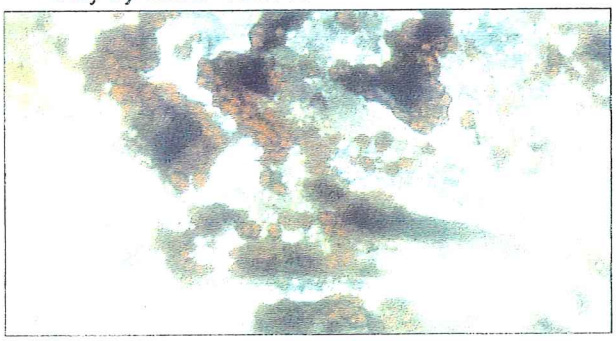

Fig 3.22 Hematite and kaolinite, surface residues of alteration - rock 7.

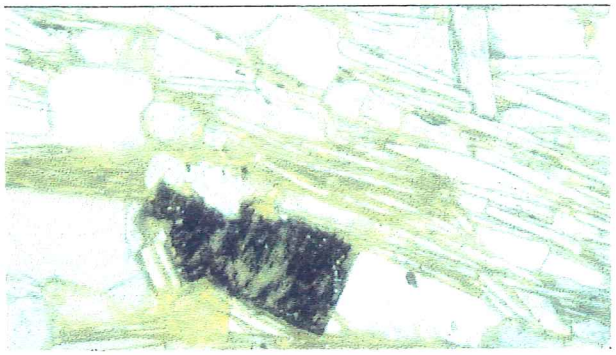

Fig 3.23 Highly altered pyrite, with goethite staining along cleavages and boundaries of muscovite - rock 3.

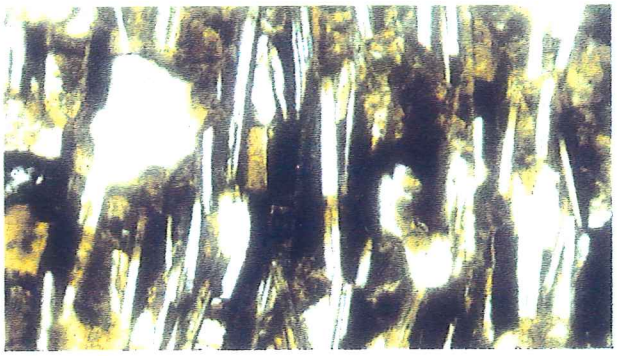

Fig 3.24 Widespread iron staining developed in leached environment - rock 4.

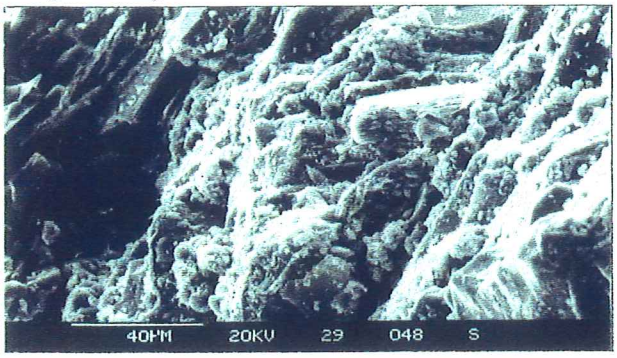

Fig 3.25 Host rock alteration with slight jarosite coating - rock 6.

Fig 3.26 Alteration of biotite to K leached end member - rock 1.

Section 3B

Laboratory studies of tailings samples

Investigations of the tailings were undertaken to discover the nature and extent of sulfide weathering, along with the nature and extent of non-equilibrium reactions such as silicate dissolution and replacement. Additionally the presence and identification of both primary and secondary minerals provided greater insight into the future geochemical evolution of the tailings. In response to the need to predict the potential for release of acid drainage from the tailings dam, a series of predictive tests and acid-base accounting procedures were undertaken. The objectives of the acid generating and neutralising predictive tests were to assess the potential for the mine waste to generate acid. A summary of the results obtained is presented in Table 3.7, with a description of the methods used available in Appendix E.

Tailings Classification

Samples for studies of the tailings were obtained from a site adjacent to hole 4 and based on observations and laboratory measurements obtained from this study the tailings profile (hole 8) can be classified into 4 main zones,

A) 0-1.37m

This is a region of strong oxidation, sulfide depletion, precipitation of insoluble sulfates and depletion of soluble salts. The lower level of this zone is bounded by a series of cemented layers present over a depth of 40 cm, each layer approximately 0.5-1.1cm thick .

B) 1.37-approx 12m

Within this zone the degree of oxidation is less due to the lack of oxygen. The material shows a profile of decreasing oxidation, interrupted by layers of oxidised material which were produced during breaks in deposition, when the surface was exposed to the atmosphere. These are considered to be palaeosurfaces. This zone may be subdivided into 2 regions on the basis of leaching and accumulation of soluble salts.

i) 1.37-approx. 9m

Concentrations of soluble salts within this region are relatively low, but increase slowly with depth.

ii) 9- approx. 12m

At this depth in the tailings, high levels of soluble salts occur. Heavy metal salts have possibly leached from the highly oxidised zone above and precipitated at depth as the solution became saturated.

Table 3.7 SUMMARY OF TAILINGS GEOCHEMISTRY

DEPTH (m)	Sample	p pH	% S (A)	%S T 1	%S T 2	%S (C)	%S (B)	% S (D)	APP (B)	AC	NNP (A)	NNP (B)	ini pH	NAP
										All quantities expressed in CaCO3 equi/tonne				
0.65-0.70	brownish yellow medium fine sand	4.25	1.00	0.31	0.22	0.69	0.09	0.22	2.8	2.8	-28	0	2.75	12
1.05-1.07	pale yellow silt layer	4.72	0.54	0.04	0.04	0.50	0.01	0.04	0.2	35.0	18	35	3.77	5
1.17-1.22	cemented layer	3.60	0.45	*	*	*	*	*	0.0	10.0	-4	10	3.15	10
1.24-1.3	cemented layer	3.75	0.43	0.02	0.02	0.41	0.00	0.02	0.0	20.0	7	20	3.52	5
1.54-1.59	top of grey medium sand region	3.93	2.75	1.45	0.60	1.30	0.85	0.60	26.6	70.1	-16	44	2.38	57
2.08-2.17	grey loamy medium-fine sand	3.89	0.95	0.55	0.16	0.40	0.39	0.16	12.2	4.7	-25	-7	2.73	21
2.48-2.55	yellow-grey loamy medium-fine sand	3.98	2.02	1.79	0.64	0.23	1.15	0.64	35.9	5.6	-58	-30	2.30	46
2.76-2.85	olive grey fine sand	4.57	1.17	0.50	0.23	0.67	0.27	0.23	8.4	5.8	-31	-3	2.65	22
3.69-3.76	dark grey loamy medium sand	4.00	4.39	4.58	1.66	0.00	2.92	1.66	91.3	4.9	-132	-86	2.15	102
4.33-4.41	olive loamy fine sand	3.88	1.68	1.60	0.52	0.08	1.08	0.52	33.8	3.4	-49	-30	2.33	36
4.90-4.50	dark olive grey medium sand	4.50	1.86	0.75	0.33	1.11	0.42	0.33	13.1	6.4	-52	-7	2.25	46
6.49-6.59	grey to light brown loamy fine sand	4.00	0.62	0.29	0.05	0.33	0.24	0.05	7.5	2.3	-17	-5	2.75	15
6.87-6.91	brown loamy fine sand	4.22	0.34	0.19	0.02	0.15	0.17	0.02	5.4	45.0	34	40	3.14	10
7.02-7.05	grey fine loamy sand	3.33	0.71	0.64	0.03	0.07	0.61	0.03	19.0	25.0	3	6	*	*
7.27-7.34	grey to dark grey loamy fine sand	3.75	0.68	0.18	0.05	0.50	0.13	0.05	4.1	1.7	-20	-2	2.70	18
7.97-8.05	olive brown loamy fine sand layer	3.80	0.88	0.33	0.19	0.55	0.14	0.19	4.4	2.5	-25	-2	2.59	20
8.24-8.35	olive-olive gray loamy fine sand	4.23	0.98	0.62	0.21	0.36	0.41	0.21	12.8	5.0	-26	-8	2.88	15
9.68-9.77	dark grey silt	3.71	0.53	0.62	0.02	0.00	0.60	0.02	18.8	2.5	-14	-16	2.79	14
10.45-10.52	dark olive grey fine sand	4.31	1.68	1.13	0.37	0.55	0.76	0.37	23.8	3.6	-49	-20	2.49	36
10.93-10.95	brown silt	3.49	0.91	0.22	0.03	0.69	0.19	0.03	5.8	35.0	7	29	3.15	10
11.09-11.11	dark grey medium sand	3.84	1.84	1.17	0.35	0.67	0.82	0.35	25.6	45.0	-12	19	2.48	38
11.65-11.75	grey loamy fine sand	3.81	0.92	0.55	0.05	0.37	0.50	0.05	15.6	2.3	-26	-13	2.66	20
12.10-12.12	dark grey loamy fine sand	3.27	0.93	0.62	0.16	0.31	0.46	0.16	14.4	20.0	-9	6	2.61	20
12.52-12.57	dark grey medium sand	4.00	2.18	1.48	0.43	0.70	1.05	0.43	32.8	35.0	-33	2	2.40	44
12.75-12.8	interbanded grey sand and silt	3.75	0.72	0.55	0.14	0.17	0.41	0.14	12.8	30.0	8	17	2.95	12
14.00-14.50	grey to light grey loamy fine sand	3.81	1.45	1.03	0.29	0.42	0.74	0.29	23.1	35.0	-10	12	2.42	33
17.52-17.57	tailings base - grey loamy fine sand	3.43	0.09	0.00	0.00	0.09	0.00	0.00	0.0	15.0	12	15	3.70	5
17.79-17.85	redoximorphic accumulation zone	3.57	0.13	0.00	0.00	0.13	0.00	0.00	0.1	40.0	36	40	3.98	5

KEY p pH = paste pH, %S (A) = % total S, %S T1 = %S treatment 1, %S T2 = %S treatment 2, % S (C) = % sulfate, %S (B) = % sulfide, %S (D) = residue S%, APP (B) = APP (total S%), NNP (A) = NNP (total %S), NNP (B) = NNP (sulfide %), ini pH = initial pH,

C) 12m - approx 18m

This section of the tailings profile has presumably been permanently below the water table, which was detected at 12-12.5m depth. Here oxygen is excluded from the system, the sulfides present are in pristine condition (excluding at palaeosurfaces), and there are low concentrations of soluble salt presumably due to through-flow of water and leaching. Sulfate-reducing bacteria (SRB) were detected in the tailings at the top of the water table (12-12.5m). The lack of SRB below this level within the tailings is probably due to the fact that bacteria at the ground water surface would be utilizing the leached sulfate, thus restricting of the quantity available at depth.

D) 18m+

This material represents the soil horizon on the original landscape below the tailings. Redoximorphic depletion and accumulation zones have developed in response to the actions of Sulfate Reducing Bacteria (SRB). These are simply regions of iron oxides and oxyhydroxides concentration or removal. Prior to deposition of the tailings, the soils would have been oxidised resulting in the development of goethite and ferrihydrite accumulations identified through XRD as a redoximorphic accumulation zone. During the subsequent deposition of the tailings and the prevailing anaerobic conditions, SRB have become active. The SRB present utilised SO_4^{2-} present in the soil, forming sulfides, additionally the Fe^{3+} from iron oxides and oxyhydroxides are put to use in the formation of iron sulfides. The utilization of the iron oxides and oxyhydroxides in upper portions of the redoximorphic accumulation has caused the development of a redoximorphic reduction zone.

Photos of the tailings cores (hole 8) obtained during sampling can be seen in Fig 3.27.

Tailings Mineralogy and Physical attributes

Based on the XRD and XRF analysis summarised in Tables 3.8 and 3.9, certain gangue minerals are continuously present in varying degrees throughout the profile. These include, quartz, anorthite, albite, clinochlore, vermiculite, phlogopite and muscovite. Tremolite is also present in some different samples. The variations are due to differences in the type of ore being processed at the time. Primary sulfides are also present below the highly oxidised near surface region. The sulfide type gives an indication of the degree of alteration. Within the top highly oxidised zone, only minor quantities of sulfide exist as pyrite. Directly below this zone, pyrite increases and pyrrhotite, the most susceptible of common sulfides to oxidation, is only slightly altered. Other minor sulfides observed at depth include sphalerite and chalcopyrite.

a) depth as marked, zone A

b) depth as marked, zone A--Bi

c) depth as marked, zone Bi

d) depth as marked, zone Bii

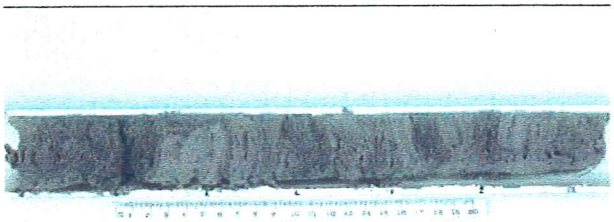

e) depth as marked, zone C

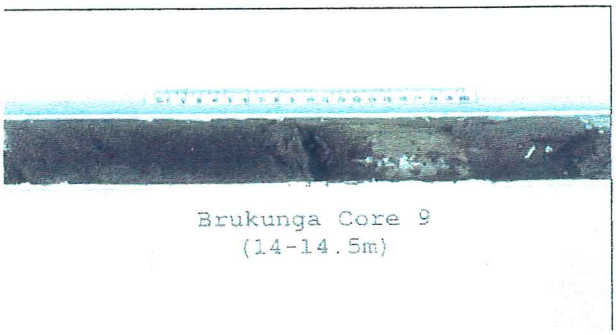

f) depth as marked, zone C

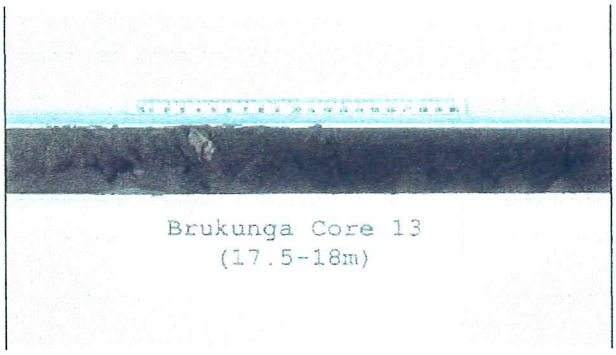

g) depth as marked, zone C

h) depth as marked, close up of tailings base, zone C-D

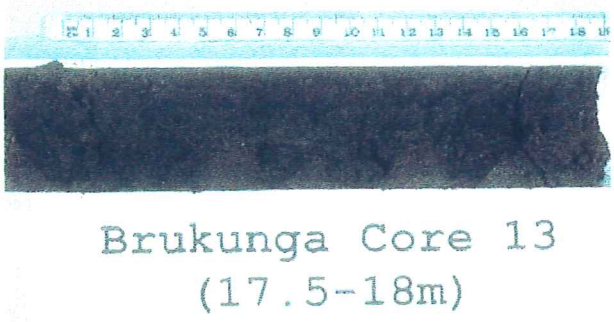

i) depth as marked, close up of redoximorphic depletion and accumulation regions, zone D

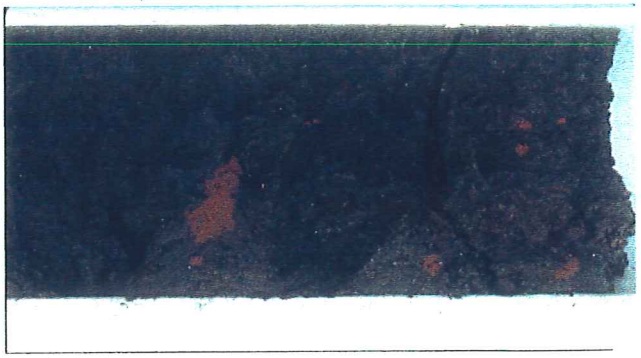

j) close up of redoximorphic accumulation region, showing iron oxyhydroxides mottles, zone D

Fig 3.27 cores taken from Brukunga tailings dam, and their classified zones.

Table 3.8 SUMMARY OF XRD RESULTS FOR TAILINGS (hole 8)

Depth (m)	sample	quartz	mus- -covite	phlog- -opite	albite	anor- -thite	clino- -chlore	vermic- -ulite	pyrite	pyrrho- - tite	sphale- - rite	trem- -olite	gypsum	berth- - ierine
0.65-0.70	brownish yellow medium fine sand	X	X	X	X	X	X						X	
0.98	orange medium sand layer	X	X	X	X	X	X							
0.99	pinkish grey silt region	X	X	X	X	X	X						X	
1.03	brown silt layer	X	X	X	X	X	X		X					
1.04	cemented layer	X	X	X	X	X		X	X					
1.06	pale yellow silt layer	X	X	X	X	X			X					
1.09	cemented layer	X	X	X	X	X	X		X					
1.13	cemented layer	X	X	X	X	X		X					X	
1.24	cemented layer	X	X	X	X	X	X		X				X	
1.28	light grey-yellow medium sand layer	X	X	X	X	X	X		X				X	
1.29	orange medium sand layer	X	X	X	X	X	X		X				X	
1.34	cemented orange medium sand layer	X	X	X	X	X		X	X				X	
1.37	cemented boundary layer	X	X	X	X	X	X	X				X	X	
1.38	light grey yellow layer	X	X	X	X	X		X	X				X	
1.39	top of dark grey fine-medium sand region	X	X	X	X	X	X		X	X			X	
1.41	base of dark grey fine medium sand region	X	X	X	X	X	X		X	X	X	X	X	
1.44	grey medium sand region	X	X	X	X	X	X		X	X	X			
1.445	grey fine sand-silt layer	X	X	X	X	X	X		X	X	X		X	
1.45	banded light grey and grey silt layer	X	X	X	X	X	X		X	X	X			
1.48	grey medium sand layer	X	X	X	X	X	X		X	X			X	
1.49	banded light grey and grey silt layer	X	X	X	X	X	X		X	X			X	
1.53	top of grey medium sand region	X	X	X	X	X	X		X	X			X	
1.58	base of grey medium sand region	X	X	X	X	X	X		X	X			X	
2.08-2.17	grey loamy medium-fine sand	X	X	X	X	X	X		X	X				
2.48-2.55	yellow-grey loamy medium-fine sand	X	X	X	X	X	X		X	X				
2.76-2.85	olive grey fine sand	X	X	X	X	X	X		X	X				
3.69-3.76	dark grey loamy medium sand	X	X	X	X	X	X		X	X				
4.33-4.41	olive loamy fine sand	X	X	X	X	X			X	X				
4.9-5	dark olive grey medium sand	X	X	X	X	X	X		X	X	X			
6.49-6.59	grey to light brown loamy fine sand	X	X	X	X	X	X		X	X				
7.04	grey fine loamy sand	X	X	X	X	X	X		X	X				
7.27-7.34	grey to dark grey loamy fine sand	X	X	X	X	X	X		X	X		X		
7.97-8.05	olive yellow-olive brown loamy fine sand layer	X	X	X	X	X	X		X	X				
9.68-9.77	dark grey silt	X	X	X	X	X			X	X				
10.45-10.52	dark olive grey fine sand	X	X	X	X	X	X		X	X		X		
10.94	brown silt	X	X	X	X	X	X		X	X		X		
11.1	dark grey medium sand	X	X	X	X	X	X		X	X	X	X		
11.65	grey loamy fine sand	X	X	X	X	X	X		X	X				
12.05	very dark grey-brown silt	X	X	X	X	X	X		X	X		X		
12.09	dark grey loamy fine sand	X	X	X	X	X	X		X	X				
12.15	dark olive grey loamy fine sand	X	X	X	X	X	X		X	X				
12.21	dark-very dark grey loamy fine sand	X	X	X	X	X	X		X	X				
12.54	dark grey medium sand	X	X	X	X	X	X		X	X		X		
12.77	interbanded grey sand and silt	X	X	X	X	X	X		X	X		X		
14.25	grey to light grey loamy fine sand	X	X	X	X	X	X		X	X				
17.52	tailings base - grey loamy fine sand	X	X	X	X	X	X							
17.73	redoximorphic depletion zone	X	X	X	X	X		X						X
17.85	redoximorphic accumulation zone	X	X	X	X			X						X

Depth (m)	sample	ferri- - hydrit	jaro- - site	chloro- - apatite	stren- - gite	cove- - llite	woodhi - site	hydrobs aluminit	roze - - nite	pyro- - chroit	peri- - clase	goeth- - ite	kaol - - mont	
0.65-0.70	brownish yellow medium fine sand	X	X	X	X									
0.98	orange medium sand layer	X		X										
0.99	pinkish grey silt region	X	X											
1.03	brown silt layer		X											
1.04	cemented layer	X	X											
1.06	pale yellow silt layer	X	X											
1.09	cemented layer	X	X											
1.13	cemented layer	X	X	X										
1.24	cemented layer	X	X			X								
1.28	light grey-yellow medium sand layer	X	X											
1.29	orange medium sand layer	X												
1.34	cemented orange medium sand layer	X	X			X								
1.37	cemented boundary layer	X	X											
1.38	light grey yellow layer		X											
1.39	top of dark grey fine-medium sand													
1.41	base of dark grey fine medium sand						X							
1.44	grey medium sand region													
1.445	grey fine sand-silt layer													
1.45	banded light grey and grey silt layer						X							
1.48	grey medium sand layer						X							
1.49	banded light grey and grey silt layer						X							
1.53	top of grey medium sand region				X		X							
1.58	base of grey medium sand region						X							
2.08-2.17	grey loamy medium-fine sand						X							
2.48-2.55	yellow-grey loamy medium-fine sand													
2.76-2.85	olive grey fine sand						X							
3.69-3.76	dark grey loamy medium sand				X									
4.33-4.41	olive loamy fine sand			X										
4.9-5	dark olive grey medium sand													
6.49-6.59	grey to light brown loamy fine sand													
7.04	grey fine loamy sand													
7.27-7.34	grey to dark grey loamy fine sand							X						
7.97-8.05	olive yellow-olive brown loamy fine sand		X				X							
9.68-9.77	dark grey silt			X					X	X	X			
10.45-10.52	dark olive grey fine sand			X						X				
10.94	brown silt				X			X						
11.1	dark grey medium sand										X			
11.65	grey loamy fine sand							X	X		X			
12.05	very dark grey-brown silt													
12.09	dark grey loamy fine sand			X										
12.15	dark olive grey loamy fine sand			X										
12.21	dark-very dark grey loamy fine sand			X				X						
12.54	dark grey medium sand				X			X						
12.77	interbanded grey sand and silt										X			
14.25	grey to light grey loamy fine sand			X	X			X						
17.52	tailings base - grey loamy fine sand													
17.73	redoximorphic depletion zone	X										X	X	
17.85	redoximorphic accumulation zone	X										X	X	

Table 3.9 XRF RESULTS FOR TAILINGS (hole 8)

Sample	SiO2 %	Al2O3 %	Fe2O3 %	MnO %	MgO %	CaO %	Na2O %	K2O %
Cemented Layer 96cm	66.7	15.3	2.23	0.049	2.8	3.02	2.12	2.94
Cemented Layer 109cm	56.7	15.3	9.41	0.049	2.7	2.06	1.73	3.51
Cemented Layer 114cm	55.2	14.95	7.96	0.066	2.9	3.4	2.05	3.22
127cm (10cm above boundary)	61.6	15.3	4.25	0.079	3.2	2.75	1.71	3.52
Boundary Cemented Layer 137cm	57.3	14.97	6.75	0.067	3.4	2.98	1.83	3.03
147cm (10cm below boundary)	60.4	16.9	5.1	0.098	3.3	2.71	1.77	3.52
Depth 3.69 - 3.76	55.7	15.7	10.91	0.078	2.9	1.87	1.3	3.41
Depth 6.87 - 6.91	62.6	17.8	2.27	0.127	3.4	3.45	2.3	3.53
Depth 9.68 - 9.77	63.4	17.4	2.27	0.112	3.7	3.22	2.5	3.6
Depth 11.09 - 11.11	62.2	15.8	5.42	0.104	3.3	3.15	2	3.32

Sample	TiO2 %	P2O5 %	SO3 %	Ba ppm	Ce ppm	Co ppm	Cr ppm	Cu ppm
Cemented Layer 96cm	0.7	0.182	0.72	1451	81	<6	89	60
Cemented Layer 109cm	0.57	0.474	2.68	2906	56	<6	91	32
Cemented Layer 114cm	0.61	0.347	4.68	2868	87	<6	106	31
127cm (10cm above boundary)	0.72	0.165	1.96	3418	139	<6	87	37
Boundary Cemented Layer 137cm	0.71	0.183	3.66	2853	144	<6	119	51
147cm (10cm below boundary)	0.71	0.147	0.81	3490	122	<6	96	44
Depth 3.69 - 3.76	0.63	0.132	10.43	5202	145	31	111	84
Depth 6.87 - 6.91	0.64	0.159	0.95	3147	72	<6.	107	37
Depth 9.68 - 9.77	0.66	0.146	1.32	2584	74	13	120	40
Depth 11.09 - 11.11	0.76	0.152	4.39	2912	129	6	118	42

Sample	Ga ppm	Zn ppm	Ni ppm	Pb ppm	Rb ppm	Sr ppm	Th ppm	U ppm
Cemented Layer 96cm	22	27	24	178	139	159	33	19
Cemented Layer 109cm	27	22	< 9	107	178	171	42	11
Cemented Layer 114cm	27	66	< 9	182	149	192	52	19
127cm (10cm above boundary)	22	104	< 9	168	165	162	35	13
Boundary Cemented Layer 137cm	24	116	16	176	142	155	33	<10
147cm (10cm below boundary)	27	1064	53	195	164	167	36	17
Depth 3.69 - 3.76	31	1113	53	275	149	159	45	16
Depth 6.87 - 6.91	28	236	13	124	175	213	53	24
Depth 9.68 - 9.77	31	375	<9.	117	170	176	55	23
Depth 11.09 - 11.11	28	818	25	212	145	172	50	25

Measurements of void ratio and porosity along with wet, dry and particle density were undertaken on the tailings materials by members of the soil engineering group. A summary of the results obtained is shown in Table 3C.1 - Appendix C2. Profiles of these attributes can be seen in Figs 3C.6, 3C.7 & 3C.8 - Appendix C2. A decrease in void ratio and porosity with depth exists, due to compaction occurring during the continuous deposition of tailings. Particle density is equivalent to the specific gravity of minerals present. The profile is very similar with depth indicating comparable waste was deposited through time. Wet and dry bulk density shows density of particles with depth ie. packing. The oven dried samples showed slight increase with depth due to compaction, whereas wet density showed large enhanced increases due to the added water content.

Tailings Geochemistry

The geochemistry of the tailings (Table 3.7) is influenced by the oxidation of the sulfides present, the amount of acid produced, and the neutralising reactions that take place in response to this.

The acid-producing reactions include the oxidation of pyrite (eq 3.1), sulfur (eq 3.22), and pyrrhotite (eq 3.3), along with the subsequent formation of secondary minerals iron-oxyhydroxides (eq 3.18) and jarosite (eq 3.15). Additionally the alteration of jarosite to ferrihydrite when conditions alter, also adds acid to the system (eq 3.23). Thus jarosite may be regarded as a storage mechanism for acid production.

Acid neutralisation reactions can be regarded as buffering reactions. Buffering reactions that occur along the groundwater flow path affect the mobility of dissolved metals as they are transported through the mine waste and through the underlying geologic materials. The main neutralising reactions occurring within the tailings include the weathering of feldspars (eq 3.9, 3.10 & 3.11) muscovite (eq 3.16) clinochlore and biotite (eq 3.24). All eventually degrade to kaolinite.

Measured parameters of the tailings are present in figures 3.28, 3.29 and 3.30, as a function of depth (the cross hatched bar present in these profiles represents cemented layers). Fig 3.28 shows profiles of soluble salt content determined through a 1:5 dilution of tailings to water, followed by ICP analysis. This identified an accumulation zone of soluble salts above the water table. Additionally experimentally determined paste pH and initial pH are presented, with values ranging from 2-4. It should be noted that at depths below the water table, direct pH measurements into sealed cores gave pH values of 5-6. The difference between direct measurements and those after drying and resuspension can be attributed to precipitation of iron oxyhydroxides upon drying and the consequent formation of H^+, thus lowering the pH. This reaction can be represented as

$$Fe^{3+} + 3H_2O \rightleftharpoons Fe(OH)_3 + 3H^+ \qquad (3.26)$$

Fig 3.28 Tailings Soluble Salt Profiles

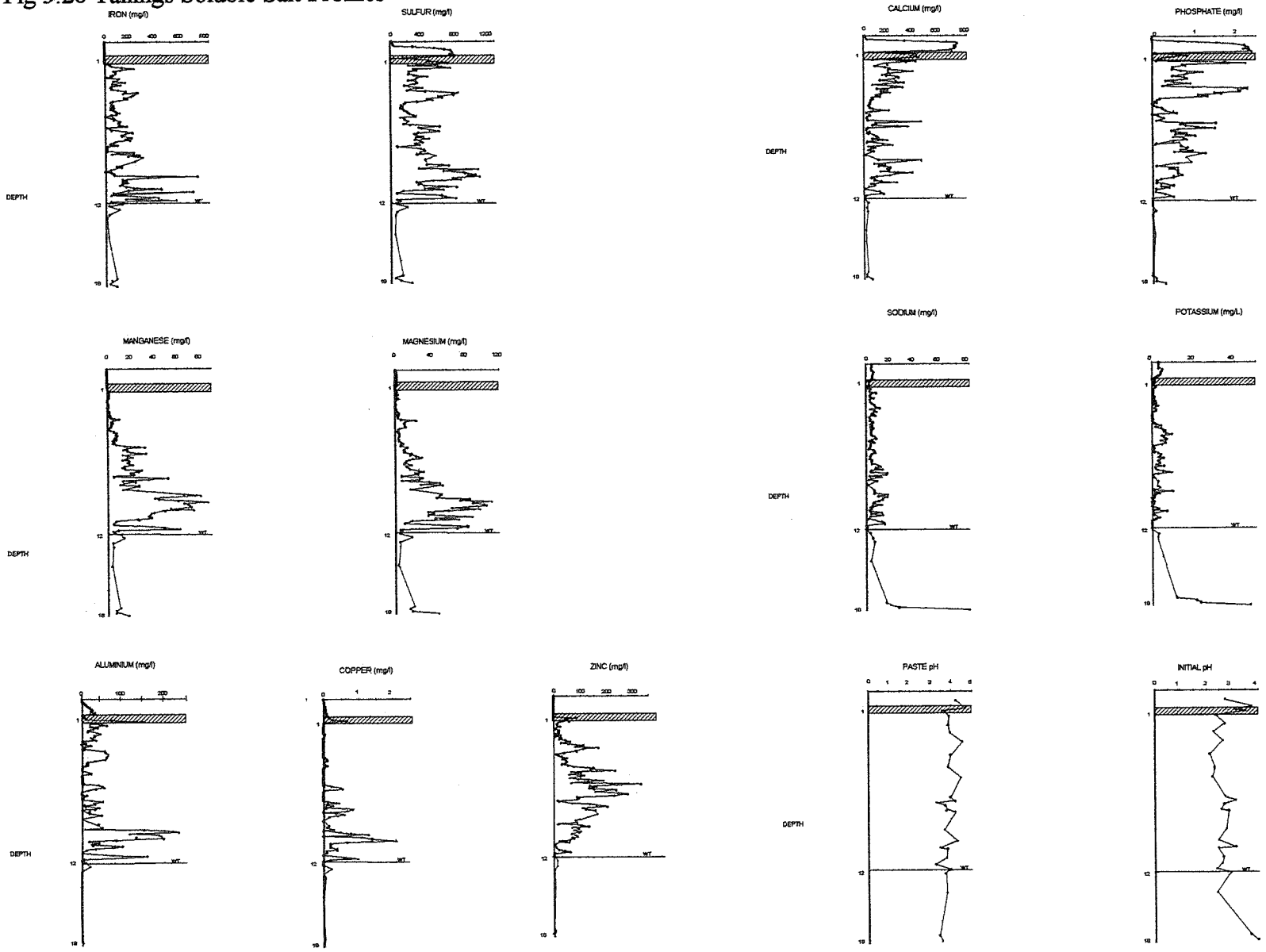

Calculations show that it only requires oxidation and precipitation of less than 2 ppm Fe^{2+} in order to release enough H^+ into pore water to decrease pH from 6 to 4. Such calculations show that the pH 5 recharge water still represents a large potential acidity if the concentration of ferrous iron is high. When the recharge water moves laterally down gradient within the ground water flow it is eventually exposed to the atmosphere as seepage through the dam wall, where the oxidation of ferrous iron causes precipitation of ferric hydroxides or jarosite. Large accumulations of iron were not observed within the water table because of this lateral through-flow.

The depth profiles of pH and soluble salts in the aqueous extracts indicate that the low pH porewater occurs throughout the unsaturated zone, while the porewater with the highest concentrations of soluble salts occurs just above the water table. Thus H^+ ions and soluble salts penetrate to similar depths, which indicates that rapid H^+ consumption reactions are not occurring and the increased concentration of ions is simply due to leaching of a front down the profile. If the soluble salts had been leached further than the low pH conditions, then effective neutralising conditions could have been hypothesized.

Morin *et al.* (1988 a,b), Morin and Cherry (1988) and Morin (1988) explain that as pyrite oxidation proceeds at the surface of tailings, the pH of acid mine drainage decreases over time in a series of steps, each of which represents the dissolution of specific buffering species present at that pH. The mineral species believed responsible for each pH plateau are

calcium-based carbonate	pH 5.5-6.4
aluminium hydroxide	pH 4.3-5
iron hydroxide and jarosite	pH 3-3.7
aluminosilicates	pH<3

XRD and optical microscopy investigations of the tailings indicate that calcite is not present in the tailings. Waste rock investigations indicate that calcite is present only in minor amounts, suggesting that any calcite originally present has been consumed during ore processing. As mentioned previously, the pH within the unsaturated zone ranges from 2-4. The highest pH of 4 corresponds with the ferrihydrite and jarosite cemented region observed in the zone directly above active oxidation (see later). pH values as low as 2 are measured down the profile, indicating that the jarosite formed in palaeosurfaces at depth is having little effect. The main potential neutralising minerals present are aluminosilicates, but their neutralising rates are slow.

Jambor and Blowes (1994) showed the comparison of chemical kinetic reaction rates for minerals as follow:

Description	**Reaction rate per unit surface area of mineral (mol $m^{-2}s^{-1}$)**
pyrite oxidation	5.12×10^{-8}
muscovite dissolution	6.32×10^{-12}
biotite dissolution	2.57×10^{-9}

Biotite is only a minor constituent of the waste rock and tailings and thus may have already been largely consumed. Dissolution of muscovite is much slower than the oxidation of pyrite and therefore has limited immediate effect on the surrounds through neutralisation.

Fig 3.29 profiles show a variety of experimentally determined attributes eg. total S, sulfide and sulfate contents of the tailings samples in the drillhole profiles. These results have been combined with analysis of the acid-consuming and producing potentials of the tailings present, to obtain a final overview of the system as the "net neutralising capacity". The total S% down the profile, along with sulfate and sulfide content gives a good indication of the conditions and reactions prevailing.

Following HCl and HNO_3 acid extractions carried out to determine sulfide and sulfate contents, significant amounts of sulfur remained in most samples. Some of these samples were investigated using the SEM/EDX and this indicated that the sulfur remaining was in the form of resistant pyrite residuals.

The initial total S% of the sulfides in tailings as they left the mill was reported as 1.4% (Blesing *et al*, 1974). Most of this is presumably sulfide, as negligible copper sulfate was used in processing (0.25 lb/tonne), and much of the processed material from the mine site would not be weathered and converted to sulfate. Consistent with this, measurements of sulfide plus residue below 1.4 m depth are approximately 1.4%.

Above 1.4m depth, extensive alteration has taken place. Rapid oxidation above the cemented layers at this depth (see below) has removed the majority of sulfides and left predominantly sulfate. Below the cemented layers, increased total S concentrations can be attributed to increases in sulfide content which is a maximum at approximately 3.7m. This increase may be attributed to irregularities in tailings deposition and variations in the ore processed at the time. This is also apparent in Fig 3.30, where XRF results reflect an increase in Fe, S, Zn, and Cu in the solid phase at about 3.7m (see Table 3.8 for detailed XRD data). Attempts were made to determine secondary biogenic origins of these sulfides through isotope analysis. These results are presented in Appendix D, but were inconclusive. Results of a lighter isotopic value compared to the ore would have verified

Fig 3.29 Tailings Geochemistry Profiles

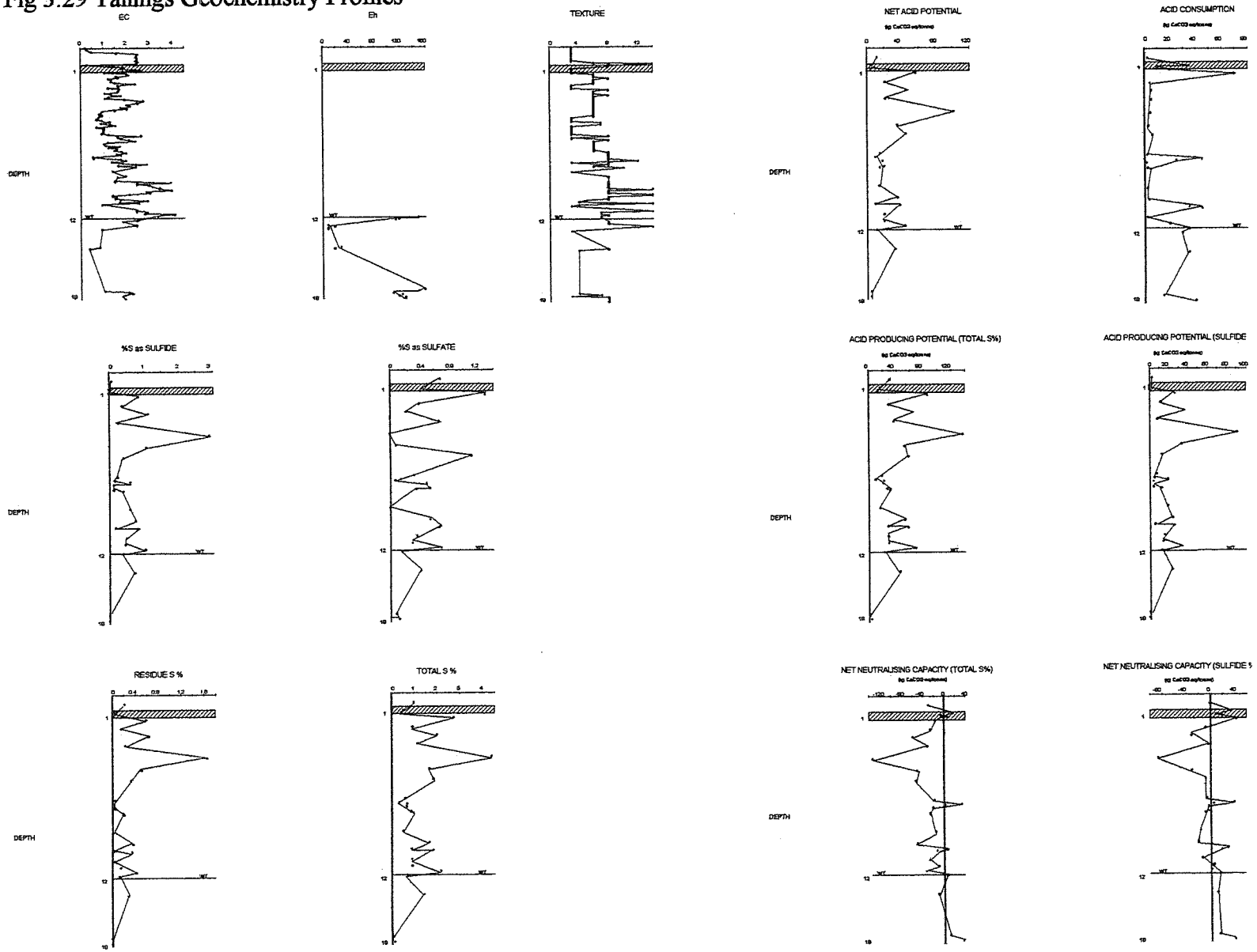

Fig 3.30 Tailings XRF Profiles

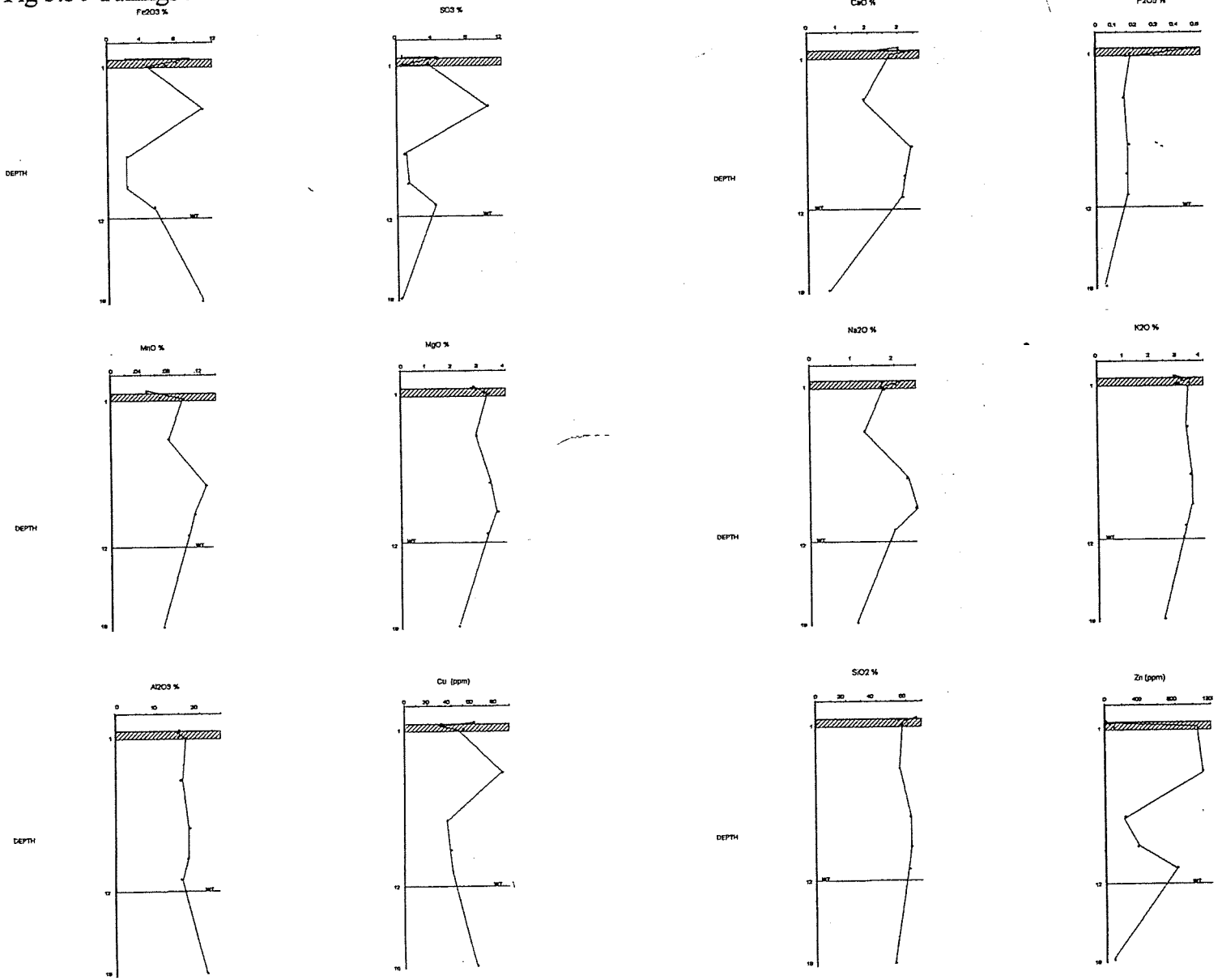

secondary biogenic formation during periods of shallower water table, however results obtained (-16) were within the variations of the ore (-12 to -18) previously determined by Seccombe *et al* (1985).

The fact that the sulfide content closely parallels the quantities originally reported, indicates that only very limited sulfide oxidation has occurred at depths below the cemented layers.

It should be noted that the minerals present in the waste rock and tailings samples are essentially the same, but in different proportions. Thus the system developing in the tailings dam is somewhat different from that in the waste rock dump. A comparison can be made looking at the results of the NNP (total S%) of the tailings and the waste rock samples. Since many of the waste rock samples have quite substantial amounts of sulfides still present, the NNP is very low (-750 kg $CaCO_3$ equiv/tonne). In comparison the lowest NNP observed in the tailings is approximately -140 kg $CaCO_3$ equiv/tonne in a zone of very high sulfide content. Generally the samples are approximately -40 kg $CaCO_3$ equiv/tonne, and where the sulfide content is low the NNP is actually positive, indicating neutralisation reactions would consume all the acid produced in the material.

Net acid production (NAP) experiments with hydrogen peroxide were also undertaken to make a comparison with acid producing potential (APP) and NNP. As can be seen by the profiles (Fig 3.29), the curves of APP based either on total S or on sulfide S closely correlate with NAP, both show variations down the profile and in acid production quantities. However the NAP experiment is designed to take into account the acid neutralisation potential also and thus should parallel the NNP, which is obviously not the case. The NNP is determined via AC-APP=NNP where AC is determined experimentally, while APP is calculated from either total %S or sulfide %S assuming a theoretical set of reaction equations.

The NNP (sulfide) is a more accurate estimate of the system, as the APP is calculated from sulfide S, rather than total S. NNP (total S) is included for comparison with rock samples. It should be pointed out that the B.C Initial Research Test that is used to determine AC, does not take into account the slow neutralising actions of aluminosilicates, which can become important over an extended period of time. A flow chart was developed using the physical and chemical attributes of the tailings to approximate the NNP. The flow chart (Fig 3C.9) is present in Appendix C2.

EC and Eh profiles are also presented in Fig 3.29. EC closely parallels soluble salt content down the profile, as would be expected. The Eh values obtained are classified by Patrick and Mahapatra (1968) as moderately reducing. Texture profiles (Fig 3.29) indicate the highly variable nature of tailings within the dam. Appendix B shows the classification scheme used for texture, with generally increased numbers representing finer grained

samples. Above the water table, a region of thin layers of fine silts are present which may have some trapping effect on the salt accumulations observed at this depth. These results were also used in a classification scheme combining EC, texture, colour and pH using the PATN classification scheme (Appendix E). The results of this classification can be seen in Fig 3C.10, Appendix C2. A detailed description of the profile including reports of these properties is present in Appendix C2.

SPECIFIC FEATURES OF THE PROFILES

1) Soluble salt accumulations and their implications

The fact that the greatest accumulations of soluble iron and sulfate soluble compounds occurs well below the current zone of sulfide oxidation indicates that the production of the iron, sulfate and heavy metals originating from sulfide oxidation and neutralising reactions, has not been constant with time. The porewaters which occur deep within the tailings represent the first water to have entered the tailings following the start of pyrite oxidation. They have leached down the profile and accumulated soluble salts produced by pyrite oxidation, which was at its greatest intensity about the time when this water first entered the tailings. The subsequent recharge waters moving through the current oxidation zone have lower concentrations of salts and thus represent a less intense oxidation period.

The highest Fe, SO_4, Mn, Mg, Al and Cu concentrations in aqueous extracts occur above the water table at about 10-12m, indicating that these ions are travelling through the tailings mass at almost the same velocity. Pyrite oxidation occurs near the tailings surface. Of the Fe^{2+} released, which is relatively mobile under low pH conditions, some will oxidise to Fe^{3+} and precipitate as iron oxyhydroxides while a certain percentage stays in the mobile state ready for leaching. The oxidation of other sulfides adds mobile Cu and Zn to the system. The neutralisation reactions taking place through the degradation of micas and feldspars in turn add Mg, Mn, Si, P, Na, Ca and Al into the system, along with many other elements. Once dissolved, these ions are then susceptible to leaching during subsequent rainfall and water infiltration, and thus are displaced further down the profile. As these constituents become saturated at depth, they accumulate through a combination of coprecipitation and absorption reactions. Only small amounts of new oxidation and neutralisation by-products have been added to the bulk of the salts as they move downward. This is partly because many ions formed subsequently have oxidised and become part of a cemented horizon.

Calculations indicate that there is approximately enough sulfate extracted into solution from samples taken at the levels of accumulation just above the water table to suggest that the majority of heavy metals are present as precipitated metal sulfates. For example, the aqueous extract at 11.8m contains 700 ppm Fe, 250 ppm Al, 120 ppm Mg, 90 ppm Mn and

500 ppm Ca (Fig 3.28). If all these cations existed as simple sulfates, then the S concentration would be 1460 ppm. This value agrees well with the measured concentration of 1200 ppm. The slight excess of cation could be caused by several factors, one of them being some substitution of hydroxyl for sulfate in the compounds.

XRD analysis was able to identify several secondary minerals in this depth range. Hydrobasaluminite ($Al_4(SO_4)(OH)_{10}.12\text{-}36H_2O$) was identified, and is suggested to be the main precipitate of Al. Rozenite ($FeSO_4.4H_2O$) was identified in samples where XRF showed peaks in Fe and S in the solid phase (Fig 3.30), while minor amounts of periclase (MgO) and pyrochroite ($Mn(OH)_2$) were responsible for accumulations of Mg and Mn. Only very small quantities of Cu exist in the system (max 2.5 ppm), although the same general increase with depth occurs (Fig 3.28). Zn has accumulated higher in the profile than the other heavy metals, and this is suggested to be due to absorption and coprecipitation with other minor metal sulfate minerals occurring at this depth (Blowes and Jambor (1990).

Ca, S and P concentrations in the soluble phase are more variable (Fig 3.28). Calcium and phosphate show decreasing concentration with depth. Large quantities of soluble calcium, phosphate and sulfur in the highly oxidised leached zone reflect the formation of gypsum ($CaSO_4$) and minor amounts of woodhouseite ($CaAl_3(PO_4)(SO_4)(OH)_6$). The phosphate content is very low in the profile with a maximum of only 2.5 ppm. The compound woodhouseite can account for some of the increases of Al, P, SO_4 and Ca observed in the highly oxidised zone, but the majority of the Ca down the profile is controlled by the precipitation of gypsum.

Cemented Layer Formation

Cemented layers have developed at the base of the oxidised zone observed in the tailings. The layers that have developed are only the preliminary stages of a hard pan. At present they exist as several thin layers of about 0.5cm thickness, ranging over an area of approximately 40cm depth (0.99-1.37m). A review of the formation of the cements and an extensive mineralogical study of the tailings dam, including XRD traces, EDX spectra and SEM micrographs, is presented in Appendix C2.

The formation of the cemented layers may have occurred in response to several different conditions taking place during the chemical evolution of the tailings mass. The initial development of minor cemented layers may have formed in response to capillary rise associated with a shallow water table, during the final stages of deposition of tailings, and the fluctuations of water associated with this. Nordstrom (1982) and Fanning and Fanning (1989) suggested a series of intermediate steps forming soluble sulfates that may occur prior to the development of the iron oxyhydroxides and soluble sulfates. Nordstrom (1982)

explained that the precursor secondary soluble sulfate minerals are most commonly formed during dry periods as evaporation promotes the rise of subsurface waters to the upper tailings by capillary action. As these waters reach the upper portion of the tailings, they become progressively more concentrated and finally precipitate various salts.

Another option is that minor cements originally developed at the plane of "zero flux", once the water table had dropped when the deposition of tailings was completed. Hillel (1971) explains that in the field, the process of evaporation hardly ever occurs independently of other processes. In general, the beginning of evaporation follows wetting, at the end of which the typical moisture profile (in the absence of a high water table condition) consists of a wet layer overlying relatively dry soil beneath. Under such conditions, two processes may be occurring simultaneously: (1) evaporation at the surface, which induces upward flow, and (2) redistribution, or internal drainage, by which water moves downward in response to gravitational and suction gradients within the deeper part of the profile. The balance between the processes occurring at the plane of zero flux would induce the precipitation of relatively soluble salts and then eventually insoluble sulfates and oxyhydroxides.

The initial cemented layer may also have developed in response to a layer with slightly more impervious texture. Whatever the origin, the development of a perched water table would enhance the formation of the cemented layers over time. This process may be still occurring today, resulting in the development of a more impervious layer to both water and oxygen, thus reducing movement of the oxidation front.

Two of the cemented layers, one at 1.04m and the other at 1.37m at the boundary between oxidised and predominantly unoxidised material, were selected for detailed analysis.

1.04m depth - Strongly cemented minor hard pan

SEM/EDX investigations indicate the cements present are a combination of ferrihydrite (Fig 3.31a), jarosite and schwertmannite (Fig 3.31b). Schwertmannite is present only as small groups of crystals, unlike the jarosite and ferrihydrite which make up the bulk of the material. XRD analysis confirm the presence of ferrihydrite and jarosite. K-alpha X-ray imaging was undertaken on this cemented layer (Fig 3.32). Large concentrations of Fe and minor S occur in the centre of the layer, corresponding to decreased amounts of Al and Si. The K-alpha image for the cemented layer at 1.04m indicates it is not a major region for absorption of cations leached from shallower regions. Also at this depth XRD indicated the presence of pyrite but it was not detected by SEM/EDX.

1.37m depth - Boundary cemented layer between oxidised and reduced material, forming a discrete well-developed cemented layer

The cement that makes up this layer varies in composition horizontally (Fig 3.33), which is thought to result from infiltrating water flushing material downward and depositing it in channels and spaces between skeleton grains. This would effectively plug much of the horizon. Intermittent and repetitive infiltration appears to have alternated with times of evaporation which initiated the precipitation of secondary minerals. Variations in precipitation would be simply due to the prevailing conditions of the time, how saturated the solution was with respect to each mineral, and the flow path available for its movement.

The cements present at this depth are a mixture of iron oxyhydroxides, minor jarosite and alunite, and the hygroscopic morphology of the majority of the material suggests the iron oxyhydroxide is ferrihydrite. Small areas of the layer show well-developed electron-dense but thin, platy crystals (Fig 3.34), which EDX analyses indicate they are iron oxyhydroxides, but presumably not ferrihydrite due to their distinctly different morphology (Fig 3.34a). Higher in the profile, above the cemented layer, discrete crystals of jarosite and alunite occur as coatings on grains (Fig 3.35 & 3.35a). K-alpha X-ray imaging undertaken on the boundary layer (Fig 3.36), indicated high concentrations of Fe and S. Fe and S are also present in large quantities above the layer as the material has leached down, become saturated and precipitated before reaching the discrete ferrihydrite band. A decrease in Fe and S is observed directly below the cemented boundary layer. Unlike the cemented layer at 1.04m depth, this layer also has high quantities of Al, Si, Ca & K. This indicates that the cement is acting as an entrapping material with Al, Si, Ca and K becoming incorporated into the layer probably as clays.

Vermiculite clay was also observed from XRD data on samples at this depth and additionally at 1.38m. Vermiculite does not occur elsewhere in the profile and it is thought to have migrated downward to this point where it accumulated because of the impervious nature of this cemented region. Its origin could be from wind blown soil prior to the dam being covered or from relict weathering material formed in the mine prior to mining. It could also be a residue after prolonged acid neutralisation reactions of an aluminosilicate such as clinochlore. It is the deposition of this fine colloidal clay carried down by percolating waters that acts as a obstruction in many of the pore spaces and helps to restrict the flow of mobile ions.

See Appendix C2 for details of individual mineral formation and detailed description of cemented layers within 0.98-1.37m depth range.

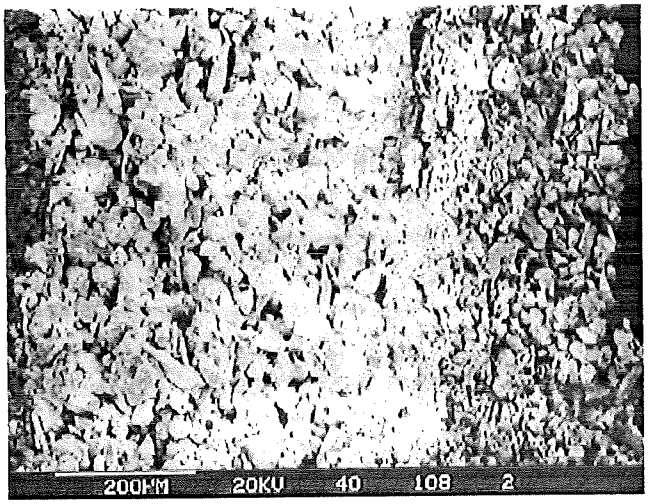

Fig 3.32a: The Backscattered Electron image of the cemented layer at 104 cm depth. The higher elevation is on the left of the image.

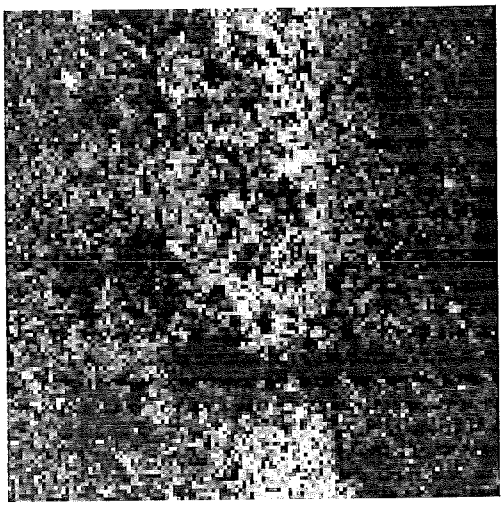

Fig 3.32b: The Fe K alpha x-ray image of the area shown in Fig. 1a. Brighter regions indicated higher Fe concentrations

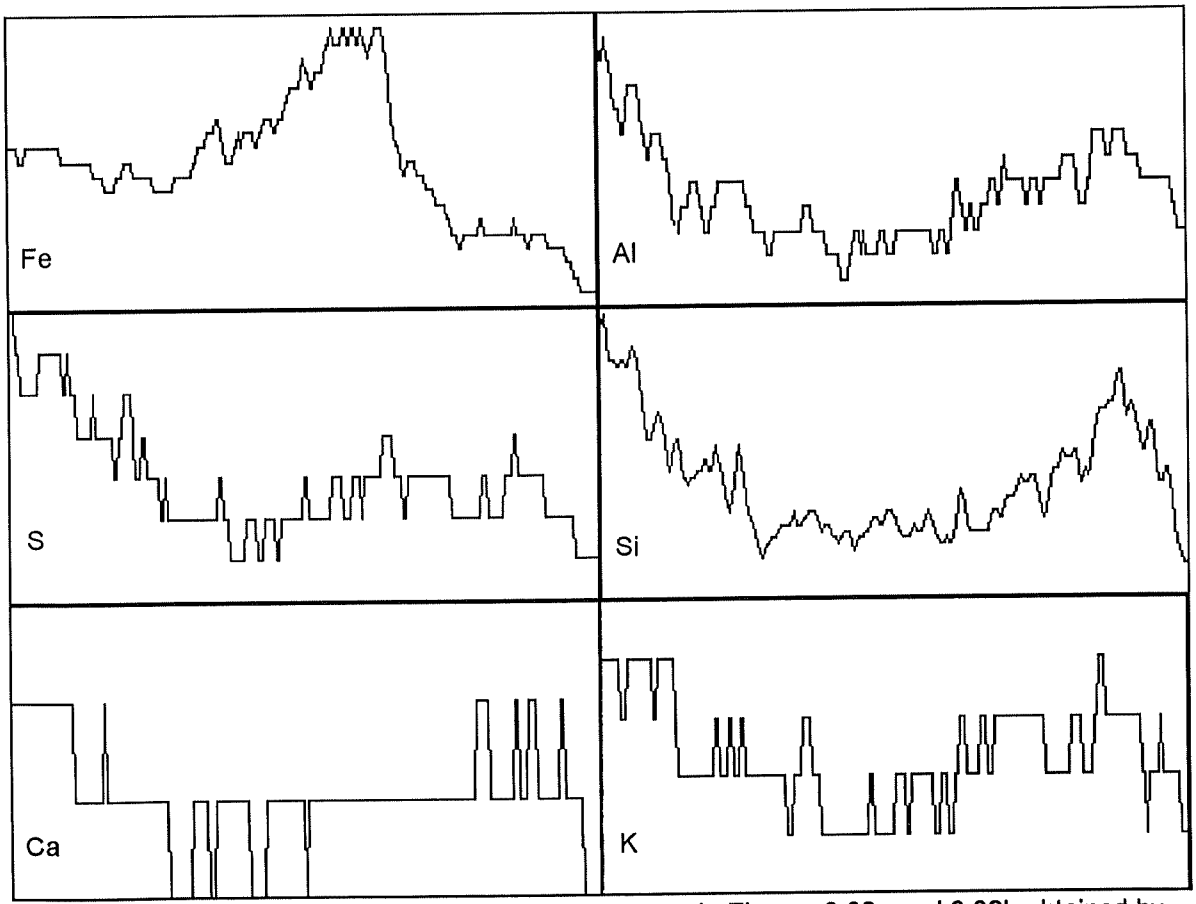

Fig 3.32c: The x-ray intensitiy profiles across the areas in Figures 3.32a and 3.32b obtained by using the average of all horizontal lines for the elements indicated. The intensities show a variation across the cemented layers. The maximum counts for each element are Fe - 20, Al - 12,S - 7, Si -44, Ca-3, and K -5.

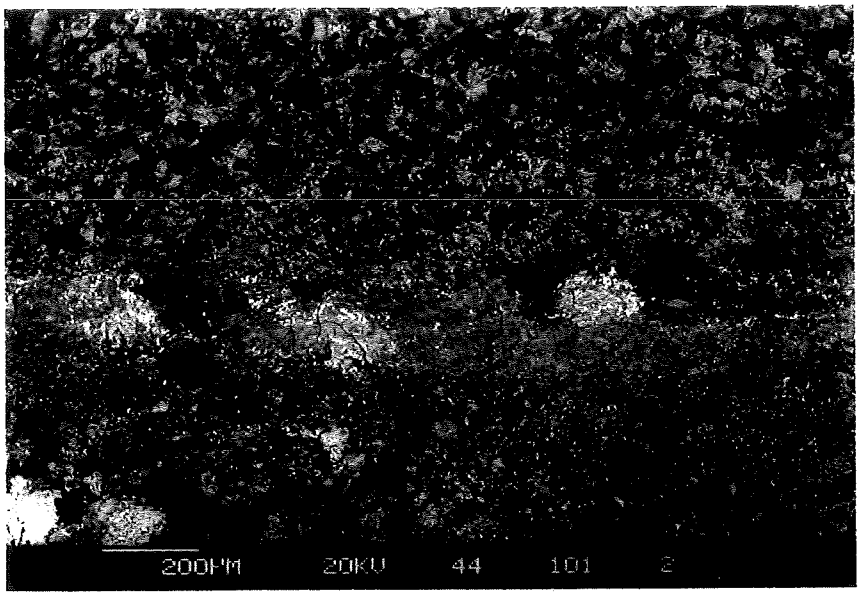

Fig 3.3 Compositional variations within the cemented boundary layer at 1.37m depth. Ferrihydrite main cement, with minor alunite and jarosite.

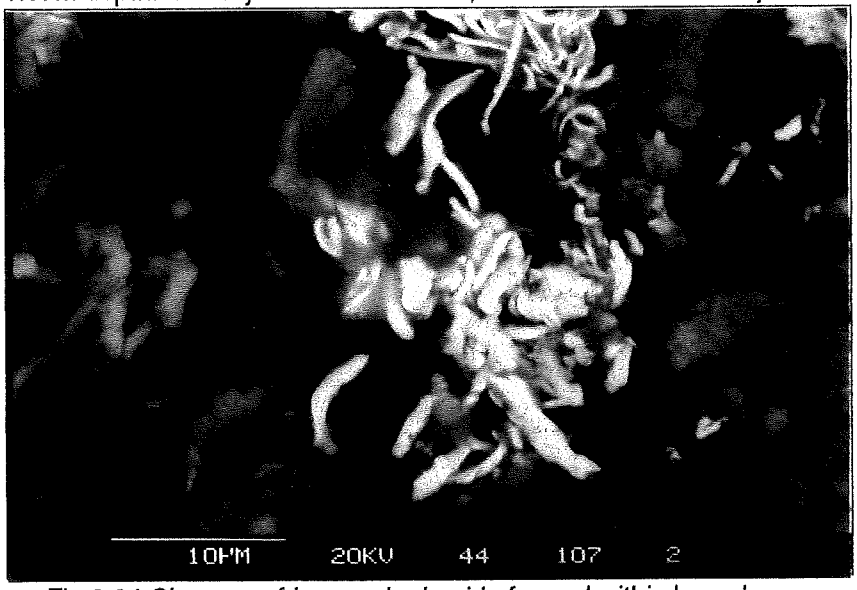

Fig 3.34 Close up of iron oxyhydroxide formed within boundary cemented layer at 1.37m depth.

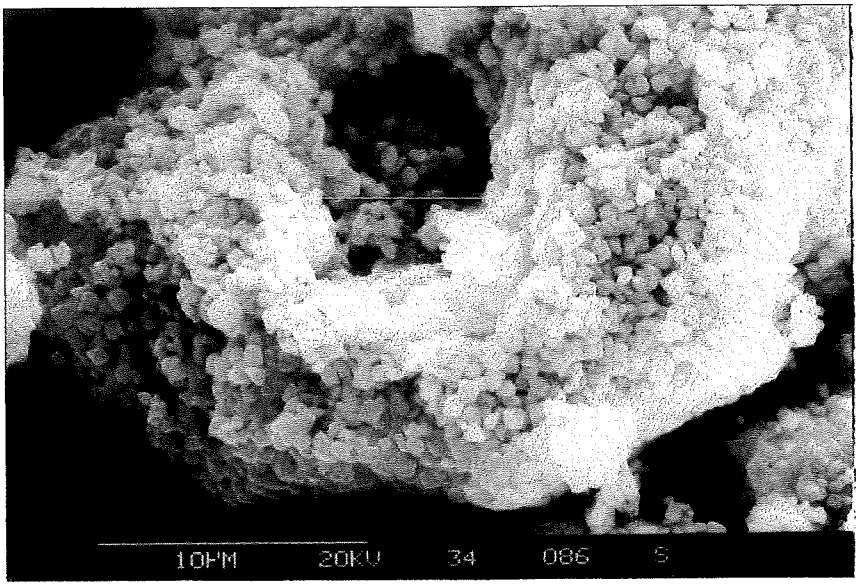

Fig 3.35 Coating of alunite and jarosite on host mineral grains above the cemented layers at 1.37m depth.

Fig 3.36a: The backscattered electron image of the cemented layer at 137 cm depth. The higher elevation is on the left. Bar scale = 400 μm.

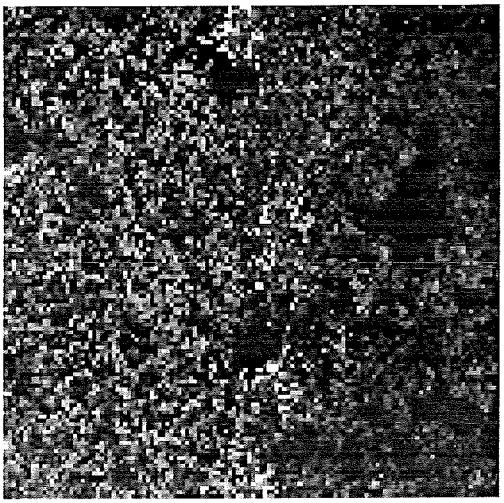

Fig 3.36b: The Fe-K alpha x-ray image of the area shown in Fig 2a. Brighter regions indicate higher Fe concentrations.

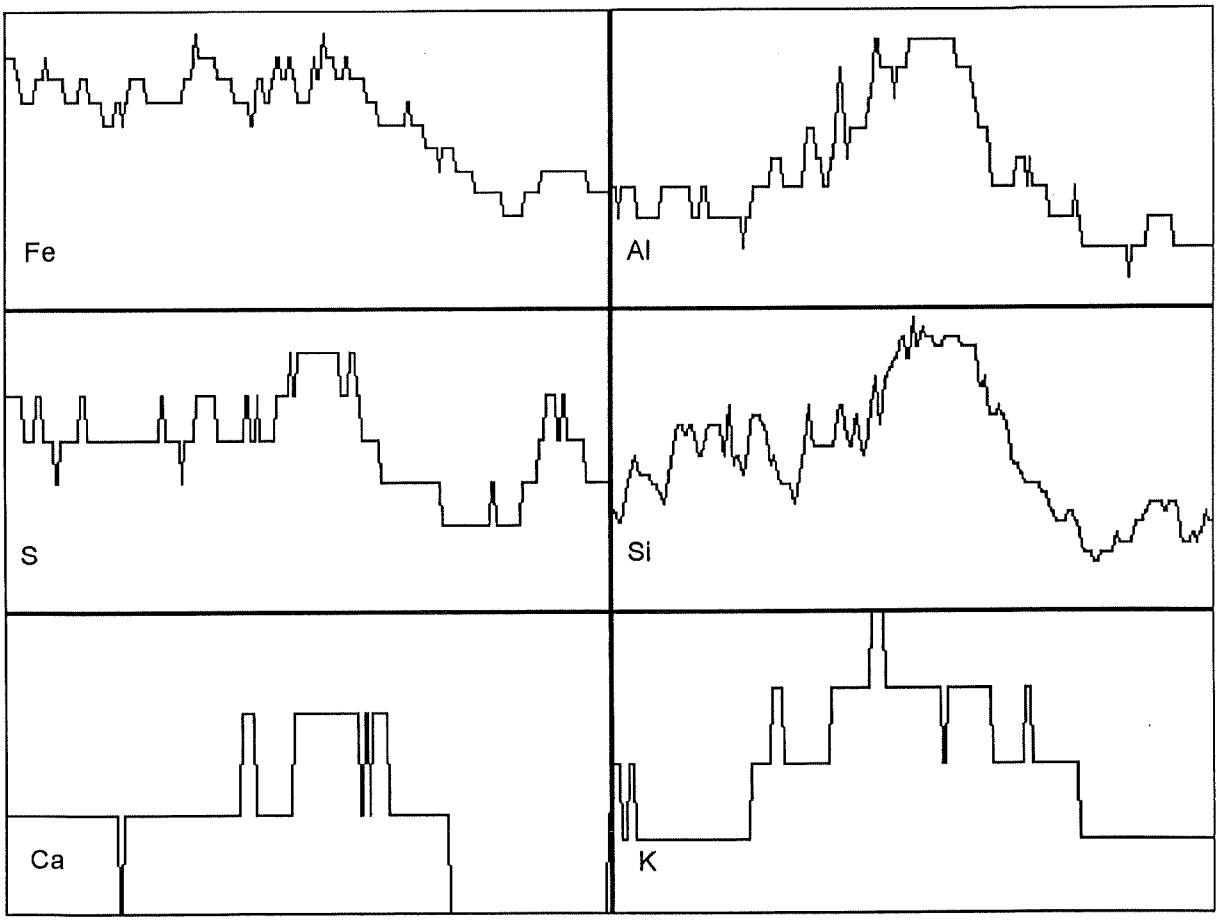

Fig 3.36c: The x-ray intensity profiles across the areas in figures 3.36a and 3.36b obtained by using the average of all horizontal lines for the elements indicated. The intensities show a variation across the cemented layers. The maximum counts for each element are Fe - 13, Al - 10, S- 7, Si - 31, Ca -3 , K - 4.

The role of cemented layers play on oxidation rate

As mentioned previously, AMD generation is presently taking place at much lower intensity than previously. The decrease in iron and sulfate production from the pyrite oxidation could be due to one of several factors or combinations of factors. As the depth of pyrite oxidation increases, the leachate approaches saturation with respect to ferrihydrite and jarosite, and precipitation of cemented layers develops.

The formation of these cemented layers has decreased oxygen penetration to a certain extent and has coated pyrite crystals with secondary minerals, so that further oxidation is inhibited. Blowes *et al.* (1991) showed that the precipitation of cemented layers decreases the rate of oxygen penetration and thus pyrite oxidation in tailings at Heath Steele mine, Canada. Using the "Readon and Moddel (1985) method", they estimate it would take 150 years to completely oxidise 1m of tailings. With a hardpan layer 15cm thick extending from 25-40cms, it would require more than 300 years to completely oxidise only the upper 40cms of the tailings. Thus the cemented layers have developed in response to the pyrite oxidation and now are helping to inhibit it.

Similar calculations can be made for the oxidation of Brukunga tailings. The position of the cemented layers corresponds with the region of active acid generation which is limited in extent. This region moves down from the surface at a rate which depends on the oxygen diffusion coefficient and the sulfide density, together with some other fixed parameters such as the density of oxygen in air and the mass ratio of oxygen required to oxidise a given mass of sulfide.

The position of the oxidation front can be calculated for uncemented tailings and compared to the position of the front which has developed. Assuming the oxygen bulk diffusivity coefficient of the dam is 5×10^{-6} $m^2 s^{-1}$, the sulfur density is 30 kgm^{-3} for approximately 2% pyrite (Ritchie, 1994), and using the equation:

Position of planar moving front within dam =

$$X^*(t^*) = \frac{(2DC_o t^*)}{(ep_{rs})}$$

$$= \frac{2 \times 5 \times 10^{-6} \times 0.265 \times (22 \times 3.15 \times 10^7)}{1.75 \times 30}$$

$$= 5.9 \text{ m depth after 22 years.}$$

Similarly the oxidation rate can be determined:

$$G(x^*t^*) = \frac{ep_s D_o C_o}{2t}$$

$$= \frac{1.75 \times 30 \times 5\times10^{-6} \times 0.265}{2 \times (22 \times 3.15\times10^{7})}$$

$$= 2.2\times10^{-7}\ kgm^{-2}s^{-1}$$

where e = mass of oxygen used per mass of reactant in oxidation reaction (1.75)

p_{rs} = sulfur density (30 kgm^{-3} for 2% pyrite)

D_o = oxygen bulk diffusivity coefficient of dam (m^2s^{-1})

C_o = concentration of oxygen is air (0.265 kgm^{-3})

t = time (s)

Thus the formation of cemented layers appears to be having an inhibiting effect on the oxidation front, reducing its movement to 1.4m depth instead of the calculated value of 5.9m for uncemented tailings. It should be noted that this model has some deficiencies in that it does not take into account the oxygen used during chemical reactions and bacterial activities, nor does it take into account variations in texture. However, these calculations give a general idea of the capacity of the cemented layers to reduce the oxidation front. This combined with the fact that the salt accumulations are at depth and do not correspond to the position of active oxidation, indicates that the oxidation occurring in the tailings dam is in fact reducing with time.

CHAPTER 4

SUMMARY AND CONCLUSIONS

Since abandonment in 1972, the Brukunga pyrite mine has produced highly contaminated, acidic drainage from the mine has been polluting the local and down stream water and soil systems, both from the tailings dam and the waste rock dumps and mine benches.

The Mine & Waste Rocks

Rock samples were graded by chemical methods in terms of their potential to generate acid mine drainage. This was related to the acid producing and neutralising minerals present and their overall significance in the system. Acid neutralising processes are fundamental in controlling the environmental effects of wastes.

Investigations of the representative rock types indicated that a combination of the physical morphology of the rock, the amount and type of sulfides and neutralising minerals present, the presence of protective coatings on grains by secondary minerals and their location in the mine dump, all play a part in the determination of the net neutralising potential of the samples and their resultant products.

Studies indicated that sulfide oxidation could lead to a variety of sulfate minerals. Jarosite was the main sulfate product, with lesser amounts of sulfur, halotrichite, kalinite and rozenite. Aluminosilicate weathering resulted predominantly in the formation of kaolinite and halloysite, however in the case of extensive weathering opal was formed. Goethite and hematite were also identified as end point weathering products.

The Tailings Dam

In an attempt to gain an overall understanding of the physical and geochemical nature of the tailings dam, core samples were collected and analysed and then compared with the results of an electromagnetic survey. The EM method was only partly successful in interpreting the measured soluble salt accumulations, because a stronger correlation with water table depth rather than electrical conductivity of samples exists. Preliminary studies

of the dam indicated that the dam is highly heterogeneous, and the water table depths change dramatically as a result of this. During deposition, the silts were deposited in the centre of the dam, with coarser material surrounding it. The fine grained impervious nature of material in the east results in a shallow water table, with the coarser material to the west being quite pervious and permeable, thus increasing the water table depth. It was shown that the marked contrast in ECa values between the eastern and western areas was not due to changes in the amount and clay content of capping material, but in fact to changes in depth and composition of groundwater.

Core logging and electromagnetic survey assisted in the selection of a site to obtain representative samples for detailed mineralogical identification and testing in the laboratory. A site adjacent to ANSTO Hole 4 was chosen and subsequently cored continuously down to the basement of the dam. Based on mineralogical observations and chemical measurements the tailings profile at this site (hole 8) was classified into 4 main zones:

A) 0-1.37m

This is a region of strong oxidation, sulfide depletion, secondary mineral precipitation of insoluble sulfates and depletion of soluble salts. The lower level of this zone is bounded by a series of cemented layers.

B) 1.37-c12m

Within this zone oxidation has decreased due to the lack of oxygen penetration. The profile which is interrupted with layers of oxidised material developed during breaks in deposition, when the surface was exposed to the atmosphere for a time (palaeosurfaces). This level may be subdivided into 2 regions on the basis of soluble salt leaching and accumulation.

C) 12m - c18m

This section of the tailings is continuously below the water table. Here the oxygen is excluded from the system and sulfides present are in pristine condition (excluding paleosurfaces). The region has low soluble salt accumulation presumably due to lateral through-flow of water and removal of salts. Sulfate-reducing bacteria (SRB) were detected in the tailings at the top of the water table (12-12.5m) and in the basement of the dam.

D) 18m+

This region encompasses the soil horizon developed prior to the deposition of the tailings. Redoximorphic depletion and accumulation zones have developed in response to SRB activity.

Throughout the profile, certain gangue minerals are present in varying degrees which reflect the type of ore being processed at the time. Primary sulfides are also present below

the highly oxidised shallow region near the surface. The sulfide type existing gives an indication of the degree of alteration with depth. The observed order of sulfide mineral removal follows the order generally observed for sulfide mineral susceptibility to oxidation. The main sulfides were pyrite and pyrrhotite, with minor amounts of sphalerite, galena and chalcopyrite.

Soluble salts and their implications

The depth profiles of pH and soluble salts in aqueous extracts of the samples indicate that low pH porewater occurs throughout the unsaturated zone, while the highest concentrations of soluble salts occur just above the water table. The fact that both H^+ and the remainder of the soluble salts have reached similar depths indicates that rapid H^+ consumption reactions are not occurring and the increased concentration of ions is simply due to leaching of a front down the profile.

Calculations indicate that there is approximately enough sulfate extracted into solution from samples taken at the levels of accumulation to suggest that the majority of heavy metals are present as precipitated metal sulfates. Some of these were identified by XRD.

The fact that the greatest accumulation of soluble iron and sulfate compounds occurs well below the current zone of sulfide oxidation indicates that AMD generation has not been constant with time. Following the initial flush of oxidation of surface material, AMD generation is currently at a much lower level.

Cemented layers formation and their effect on oxidation.

Cemented layers have developed at the base of the oxidised zone observed in the tailings. The formation of the cemented layers is having an inhibiting effect on the oxidation front, reducing its movement to 1.4m depth instead of the calculated value for uncemented tailings of 5.9m.

The formation of the cemented layers may have occurred in response to several different conditions taking place during the evolution of the tailings geochemistry. The initial development of minor cemented layers may have formed in response to capillary rise associated with a shallow water table, present during the final stages of deposition of tailings, and the fluctuations of water associated with this. Another option is that minor cements originally developed at the plane of "zero flux", once the water table had dropped after the deposition of tailings was completed. The initial cemented layer may also have developed in response to a slightly more impervious textual layer. After the initial creation, the development of a partly perched water table would enhance their formation over time. This process may be still occurring today, resulting in the formation of a more impervious

layer to both water and oxygen, thus reducing the intensity and movement of the oxidation front.

Acid production and Neutralisation

The geochemistry of the tailings that has developed is due to the oxidation of the sulfides present, the acid produced, and the neutralising reactions that take place in response to this.

Results of the experimentally determined sulfide/sulfate contents have been combined with analysis of the acid-consuming and producing potentials of the tailings present, to obtain a final overview of the system as the "net neutralising capacity". The total S% down the profile, along with sulfate and sulfide content gives a good indication of the conditions and reactions prevailing. The initial total S% of the sulfides in tailings as they left the mill was reported to be 1.4% (Blesing *et al*, 1974), and this is consistent with values of about 1.4% measured in current work for sulfides in samples below about 1.4m, and indicates that only very limited oxidation has occurred at depths below the cemented layer. Above 1.4m extensive alteration has taken place. Rapid oxidation above the cemented layers has removed the majority of sulfides and left predominantly sulfate.

It should be noted that the minerals present in the waste rocks and the tailings are essentially the same, but in different proportions, hence the system developing in the tailings is somewhat different from the waste rock dump. Since the waste rocks have quite substantial amounts of sulfides still present, the NNP is very negative, compared to the NNP observed in the tailings. Positive NNP recorded at some depths, suggest neutralisation reactions in the tailings could consume all acid produced.

Implications for the future

The waste rock dump represents a continual acid producing environment. The sheer quantities of sulfide present in some of the rocks (up to 22%) will ensure that acid production occurs for many years to come. The lack of rapid neutralising minerals enhances the problem but, the presence of slow neutralising aluminosilicates will have an effect over an extended period.

Within the tailings, the acid production due to 'surface region' oxidation is decreasing with time. The development of cemented layers at the oxidation front is inhibiting its movement and thus reducing acid production. It is postulated that the continual formation of this cemented region will produce a more impervious layer to both oxygen and water, thus forming a natural seal to the tailings.

The water continually seeping from the face of the dam carries increased concentrations of iron and other mobile heavy metals to the surface where they are exposed to oxygen. The subsequent oxidation results in the formation of large quantities of acid. Additionally, as this water moves to the front of the dam it comes in contact with the waste rocks which were used to build the dam wall. This water, along with the oxygen available in the atmosphere, rapidly oxidises the rocks, adding further acid to the system.

The combination of these two acid producing environments (waste rock dumps and tailings), represents the greatest on-going environmental threat, and reduction of this is essential. The removal of the neutralisation sludge lagoons (the by-products of the neutralisation plant in use at the mine) from the tailings surface would reduce the through-flow of water somewhat, but this only represents a small fraction. The establishment of vegetation on the entire dam (which is currently being undertaken) will reduce much of the rainfall infiltration, however it is the groundwater flowing through the tailings that represents the main input of water. Revegetation of the waste rock dumps would serve the same purpose.

Although the tailings oxidation at the surface is decreasing over time, the removal of this through-flow would further reduce the hazardous conditions prevailing. An effective mechanism of controlling the ground water flow through both the waste rock dumps and the tailings would minimise the future environmental impact due to the Brukunga Mine site.

Acid Mine Drainage (AMD) developed at the Brukunga Pyrite Mine, South Australia

Acknowledgments

Firstly, to my supervisors - Dr Arthur Fordham, Ian Hollingsworth and Dr Vic Gostin thankyou for your assistance during the year. Special appreciation to Arthur who has been a great source of equanimity throughout the year.

For the back breaking sampling at the tailings dam, recognition must go to Martin Wright and Roy Martin. Additional appreciation to Paul Peter for organising the physical attributes of the tailings material to be determined.

Thankyou to the following people for their assistance during the year both teaching and performing different skills required during my studies.

Mark Raven and Graham Riley - XRD
Paul Fazey - XRF
Stuart McClure - SEM
Jim Beatty - Total Sulfur % determination
John Coppi - photography
Santo Ragusa - bacterial information
Keith Turnbull - Sulfur isotope determination
ACU members - chemical analysis

I am very grateful to the many people who provided information during the initial stages of investigations into the rehabilitation of the mine. Many thanks to

Peter Manthey - EWS
Bob Wildy - SADME
Bob Bradshaw - former employee of Nairne Pty Ltd.
Special thanks to Peter Grindley for the extensive discussions on site.

Additionally thanks to all other members of the Minesite Group, Mineralogy Dept and Soils Dept at the CSIRO, and staff at the University of Adelaide. Special thanks to Dr Tony Milnes and Dr Rob Fitzpatrick.

To all the honours students of 1994, both at the University of Adelaide and CSIRO, thanks for all your support and for helping me enjoy this year. Thanks also to Bruce Schaefer for his last minute words of wisdom.

Additionally to my family and friends, thanks for your long distance support. Lastly, to the most important person in my life, my husband Richard, thankyou from the bottom of my heart for all the support you've given this year and holding my hand through the rough patches. Also thanks to my dog Charlie, who was always a comfort by my side during the long nights of studying.

BIBLIOGRAPHY

AGC Woodward- Clyde, 1991. Brukunga Mine site Rehabilitation, personal communication to Mr P Hill

Al, T., Blowes, D. and Jambor, J., 1994. The pore-water geochemistry of the Cu-Zn mine tailings at Kidd Creek, near Timmins, Ontario, Canada, International Land Reclamation and Mine Drainage Conference and the 3rd International Conference on Abatement of Acidic Drainage, Pittsburgh, pp208-217.

Alpers, C. and Blowes, D., 1994. Environmental Geochemistry of sulfide oxidation, *ACS symposium series* **550**. American Chemical Society Washington D.C.

Alpers, C. and Blowes, D., 1992. Environmental geochemistry of sulfide oxidation, American Chemical Soc. Washington D.C.

Armstrong, A. and Betheras, F., 1952. Nairne Pyrite deposit-Explanation, *SA Dept of Mines report*, pp 98-107.

Bain, D., 1977. The weathering of ferruginous chlorite in a podzol from Argyllshire, Scotland, *Geoderma* **17**. Elsevier Sci. Pub. Co, Amsterdam.

Bartel. O,. 1952. The Nairne Pyritic Formation, Aust, *Economic geology*. **54** pp 509-510.

Bar-Yosef, B., Barrow, N. and Goldshmid, J., (Eds) 1989. Inorganic contaminants in the vadose zone, *in* Ecological studies **74**. Springer - Verlag Berlin, printed in the USA.

Berner, R., 1984. Sedimentary pyrite formation: an update, *Geochim. Cosmochim. Acta*, **48**.

Blair, R., Cherry, J., Lim, T. and Vivyurka, A., 1980, Groundwater monitoring and Contaminant occurrence at an abandoned tailings area, Elliot Lake, Ontario, Proc. First International Conference on Uranium Mine waste Disposal, Vancouver, May 19-21 Soc. Mining Engineers, AIME, pp 411-444.

Bigham, J., Schwertmann, U. and Carlson, L., 1992. Mineralogy of precipitates formed by the biogeochemical oxidation of Fe(II) in mine drainage, *in* Skinner H and Fitzpatrick R (Ed) Biomineralisation - Processes of iron and manganese Catena Verlag, Germany.

Bigham, J., Schwermann, U., Carlson, L. and Murad, E., 1990. A poorly crystallized oxyhydroxysulfate of iron formed by bacterial oxidation of Fe(II) in acid mine water, *Geochimica et Cosmochimica Acta* **54**, pp 2743-2758.

Birnbaum, S. and Wirman, J., 1985. Sulfate-reducing bacteria and silica solubility a possible mechanism for evaporite diagenesis and silica precipitation in banded iron formation, *Can J Earth Sci.* **22**, pp 1904-1909.

Blaskett, M., 1993. Personal communication to Dr A Milnes : Registration of Interest: for engagement of a consultant to develop options for the rehabilitation of the Brukunga Minesite and tailings dam, *E & WS Dept.*

Blesing, N., Lackley, J. and Spry, A., 1974. Rehabilitation of Brukunga Mine : Nairne Pyrites Ltd, *Amdel Report* **1015**.

Blowes, D., Ptacek, C., Frind, E., Johnson, R., Robertson, W. and Molson, J., 1994. Acid-neutralisation reactions in inactive mine tailings impoundments and their effect on the transport of dissolved metals, International Land Reclamation and Mine Drainage Conference and the 3rd International Conference on Abatement of Acidic Drainage, Pittsburgh.

Blowes, D., Jambor, J., Appleyard, E., Reardon, E. and Cherry, J., 1992. Temporal Observations of the geochemistry and mineralogy of a sulfide rich mine-tailings impoundment, Heath Steele Mines, New Brunswick, *Explo. Mining Geol*, **1/3**, pp 251-264.

Blowes, D., Reardon, E., Jambor, J. and Cherry, J., 1991. The formation and potential importance of cemented layers in inactive sulfide mine tailings, *Geochimica et Cosmochimica Acta* **55**, pp 965-978. Pergamon Press plc, printed in USA.

Blowes, D. and Jambor, J., 1990. The porewater geochemistry and the mineralogy of the vadose zone of sulfide tailings, Waite Amulet, Quebec, Canada, *Applied Geochemistry* **5**, pp 327-346.

Blowes, D., Cherry, J. and Reardon, E., 1988. Field observations on the rate of Geochemical Evolution of tailings ore waters at the Heath Steele mine, New Brunswick, International Groundwater Symposium of the International Assoc. of Hydrogeologists, Canadian National Chapt, Atlanta Region, Halifax, Nova Scotia, pp 5-17.

Blowes, D., Cherry, J. and Reardon, E. 1987. The hydrogeochemisty of four Inactive tailings impoundments: Perspectives on tailings pore-water evolution, Proc., National symposium on Mining, Hydrology, Sedimentology and Reclamation, University of Kentucky, Lexington, Kentucky, pp 253-261.

Boorman, R.S. and Watson, D., 1976. Chemical processes in abandoned sulfide tailings dumps and environmental implication for Northeastern New Brunswick, *Environmental Control. CIM Bulletin*, pp 86-96.

Both, R., 1990. Kanmantoo Trough-Geology and mineral deposits, *in* Hughes F (Ed) Geology of the mineral deposits of Australia and Papua New Guinea **14**. The Australian Institute of Mining and Metallurgy.

Brinkman, R., 1979. Ferrolysis - a soil forming process in hydromorphic conditions, Centre for agricultural publishing and documentation, Wageningen.

Burns, M., 1969. The determination of pyritic sulfur in Australian coals, *Investigation Report* **82**, Divison of Mineral Chemistry, CSIRO, Australia.

Bush, K. and Markos, G., 1981. Evidence for the instability of silicate minerals in acid leach uranium mill tailings, Symposium on Uranium mill tailings management, Fort Collins, Colorado, Oct 26-27 1981, pp 473-486.

CANMET, 1988 Reactive acid tailings stabilization program (RATS), *CANMET special pub*. **SP88-3**.

Carlson, L. and Schwertmann, U., 1981. Natural ferrihydrites in surface deposits from Finland and their association with silica, *Geochimica et Cosmochimica Acta* **45**, pp 421-429.

Chalkley, M., Conard, B., Lakshmanan, V. and Wheeland, K., 1989. Tailings and Effluent Management, Proc. of the international symposium on tailings and effluent management, Halifax, Aug 20-24, 1989. Pergamon Press.

Cherry, J., Shepard, J. and Morin, K., 1982. Chemical composition and geochemical behaviour of contaminated groundwater at Uranium tailings impoundments, Society of mining engineers of AIME.

Cherry, J., Blackport, R., Dubrovsky, N., Gilham, R., Lim, T., Murray, D., Reardon, E. and Smyth, D., 1980. Subsurface hydrology and geochemical evolution of inactive pyritic tailings in the Elliot Lake Uranium district, Canada, Symposium on Uranium mill tailings management, Halifax, Aug 20-24 1980. Geotechnical Eng. Program, Civil Eng. Dept Colorado State University, pp 353-385.

Clayton, J. and Walker, W. 1981. Revegetation trials on the tailings dam, *SADME Report* .**1149**.

Coastech Manual, 1991. Acid rock drainage production manual, Prepared for *CANMET, Dept of Energy, Mines and Resources, Canada*. SSC File **0095Q.23440-9-9149.**

Coggins, C., Blowes, D. and Robertson, W., 1991. The hydrogeology and geochemistry of a nickel-mine tailings impoundment, Copper Cliff, Ontario, 2nd international conference of the Abatement of acid drainage, Montreal, Sept 1991, **4**, Nedem Mend.

Cook, P. and Walker, G., 1992. Depth profiles of electrical Conductivity from Linear Combinations of Electromagnetic Induction Measurements, *Soil Sci. Soc. Am J* **56**, pp 1015-1022.

Daily, B. and Milnes, A., 1972. Revision of the stratigraphic nomenclature of the Cambrian Kanmantoo Group, SA, *Journal of the Geological Soc. of Aust.* **19/2**.

Daily, B. and Milnes, A., 1971. Stratigraphic notes on Lower Cambrian Fossiliferous metasediments between Cambell Creek and Tunkalilla Beach in the type section of the Kanmantoo Group, Fleurieu Peninsula, SA, *Trans. R. Soc. S. Aust.* **95/4**, pp 199-214.

Dainis, I., 1993. A proposal for measuring the present impact of Brukunga acid quarry effluent on the Bremer River system, *SADME Report.*

Dainis, I., 1992. Environmental Chemistry at Brukunga, *SADME Report.*

Deer, W., Howie, R. and Zussman, J., 1966. An introduction to the rock forming minerals, William Colwes and Sons, Ltd, London.

Doepker, R., 1991. Column leach Study IV : Factors affecting the dissolution of metals from sulfidic metal mine tailings, Proc. International conf. on Abatement of Acidic Drainage, MEND, NEDEM, Montreal, pp 115-138.

Doherty, L., 1978. Rehabilitation of Brukunga Pyrite mine, *SADME Mining Resource* File **B-S-1**.

Dubrosky, N., Cherry, J., Reardon, E. and Vivyurka, A., 1984. Geochemical evolution of inactive pyritic tailings in the Elliot lake Uranium district, *Can. Geotech. J.* **22**, pp 110-128.

Dutrizac, J. and Kaiman, S., 1976. Synthesis and properties of jarosite type compounds, *Canadian Mineralogist* **14**, pp 151-158.

Environmental Geochemistry International (EGI) Pty Ltd, 1993. Rehabilitation Planning for the Brukunga Minesite and Tailings Dam, *SADME Report.*

EWS, 1988. Use of sodium Carbonate at Brukunga neutralisation plant, *Minutes forming Enclosure*. Report **139/88**.

Fanning, D. and Fanning, M., 1989. Soil - Morphology, Genesis and Classification, John Wiley and sons, Inc.

Feenstra, S., Blair, R., Cherry, J., Chakrovatti, J. and LaRocque, E. 1981. Hydrogeochemical Investigations of two inactive tailings areas in the Elliot lake Uranium District, Ontario Canada, Symposium on Uranium Mill Tailings Management, Fort collins, Colorado, Oct 26-27, 1981, pp 367-388.

Ferguson, K. and Morin, K. 1991. The prediction of Acid Rock Drainage - lessons from the Database, 2nd international conf. on the Abatement of acidic drainage Montreal Sept 1991, Nedem Mend **3**, pp 83-106.

Filion, M., Sirois, L. and Ferguson, K. 1990. Acid mine drainage research in Canada, *CIM Bulletin*, pp 33-40.

Fordham, A., 1993. Porewater Quality of uranium tailings during laboratory aging and its relation to solid phase, *Aust. J. Soil. Res.*, **31**, pp 365-390.

Fordham, A., 1990. Weathering of biotite into dioctahedral clay minerals, *Clay minerals* **15**, pp 51-63.

Fordham, A., 1990. Treatment of microanalyses of intimately mixed products of mica weathering, *Clays and clay minerals*, **38/2**, pp 179-186.

Fossing, H. and Jorgensen, B. 1989. Measurement of bacterial sulfate reduction in sediments: Evaluation of a single step chromium reduction method, *Biogeochemistry* **8**.

Gardner, W., 1965. Movement of Nitrogen in soil *in* Bartholomew W and Clark F (Eds), Soil Nitrogen, Am. Soc. Agronomy, Madison, Wisconsin.

George, R., 1967. Metamorphism of the Nairne pyrite deposit, Ph.D. thesis (unpub), The University of Adelaide.

George, R., 1969a. Sulfide-silicate reactions during metamorphism of the Nairne pyrite deposite, *Proc. Australas. Inst. Min. Metall.*, **230**.

Gilkes, R. and Little, I., 1972. Weathering of chlorite and some associations of trace elements in Permian phyllites in southeast Qlds, *Geoderma* 7.

Herbillon, A. and Makumbi, M., 1975. Weathering of chlorite in a soil derived from a chlorite schist under humid tropical conditions, *Geoderma* **13**. Elsevier Sci. Pub Co, Amsterdam.

Herbillon, A. and Nahon, D., 1988. Laterites and Laterization processes *in* Iron in soils and clay minerals. D. Reidel Publishing company.

Hillel, D., 1971. Soil and water - Physical principles and processes, *in* Kozlowski T (Ed) Physiological Ecology - A series of Monographs, Tests and Treatises. Academic Press New York and London.

Hladky, G. and Slansky, E. 1981. Stability of alunite minerals in aqueous solutions at normal temperatures and pressures, *Bull. Mineral* **104**, pp 468-477.

Holton, J. 1969. A preliminary assessment of the geology and ore reserves of the iron sulfide beds of the Nairne Pyrite member at Downer Hill, Brukunga, *BHP Report* **CR 1204**.

Horbaczewski, J. and Van Ryn, F., 1988. Geochemistry of abandoned lignite mine spoil in Texas, Mine drainage and surface mine reclamation Conf., Pittsburgh, 1988, pp 157-163.

Ivarson, K., Ross, G. and Miles, N., 1987. Microbiological transformations of iron an sulfur and their applications to acid sulfate soils and tidal marshes *in* Kittrick J, Fanning D and Hossner L (Eds), Acid sulfate weathering Soil Sci. Soc. of Am., Wisconsin.

Jackson, N., 1952. Summary of experimental work on Nairne Pyritic Ore, *Metallurgical Report* **41**, SADME, pp 123-139.

Jackson, N., 1950. Diamond drilling of Gibraltar Pyrite Deposit-Naire, *Mining Review* **90**, pp 83-86.

Jambor, J. and Blowes, D., (Eds) 1994. Short course Handbook on environmental geochemistry of sulfide mine-wastes, Mineralogical Ass. of Canada, Waterloo, Ontario.

Jambor, J. and Blowes, D., 1990. Major-element variations in the reactive sulfide-rich tailings at the Waite Amulet Minesite, Noranda Area, Quebec, Canada *in* Petruk, W., Hagni, R., Pignolet, S. and Hausen, D., (Eds), Process Mineralogy IX, pp 511-523.

Jenson, M. and Whittles, A., 1969. Sulfur Isotopes of the Nairne Pyrite deposit, SA, *Mineral Deposita*, **4**, pp 241-247.

Johnson, D., Kelso, W. and Jenkins, D. 1979. Bacterial streamer growth in a disused pyrite mine, *Environ. Pollut.* **18**, pp 107-118.

Jorgensen, B., 1978. A comparison of methods for the qualification of bacterial sulfate reduction in coastal marine sediments, *Geomicrobiology J.* **1/1**.

Kadama, H. and Ross, G., 1976. Experimental alteration of chlorite into a regularly interstratified chlorite-vermiculite by chemical oxidation, *Clays and clay minerals*, **24**. Pergamon Press.

Kelly, D., 1968. Biochemistry of oxidation of inorganic sulfur compounds by microorganism, *Aust. J. Sci.* **31/5**, pp 165-173.

Kittrick, J., Fanning, D. and Hossner, L., 1987. Acid sulfate weathering Soil Sci. Soc. of Am., Wisconsin

Kraatz, M. and Applegate, R.J., 1992. The rum jungle rehabilitation project monitoring report 1986-88: *Technical Report* . **51**. Land conservation Unit, Conservation Commission of the NT.

Lackley, J., 1976. Brukunga neutralisation pilot plant, *Amdel report*, **1096**. SADME.

LaGanza, R., 1959. Pyrite investigations at Nairne, SA., *Economic Geology* **54**, pp 895-902.

LaGanza, R., 1958. 'Origin of Nairne pyrite deposit, *Economic geology*, **54**, pp 333-335.

Lawerence, R., Poling, G., Ritcey, G. and Marchant, P., 1989. Assessment of predictive methods for thdetermination of AMD potential in mine tailings and waste rock *in* Chalkley, M., Conard, B., Lakshmanan, V. and Wheeland, K., Tailings and Effluent Management Proc. of the international symposium on tailings and effluent management, Halifax, Aug 20-24, 1989. Pergamon Press.

Lazaroff, N., Melanson, L., Lewis, E., Santoro, N. and Pueschel, C., 1985.. Scanning electron microscopy and infrared spectroscopy of iron sediments formed by Thiobacillus ferroxidans, *Geomicrobiology J.* **4/3**, pp 231-268.

Lowson, R., 1982. Aqueous oxidation of pyrite by molecular oxygen, *Chemical Review*, **82**, pp 461-493.

Markos, G. and Bush, K., 1982. Geochemical Processes in uranium mill tailings and their relationship to contaminants, International symposium on management of waste from uranium mining and milling, Albuquerque, pp 231-246.

Mason,G., 1968. Report of Nairne pyrite deposit, *SADME Report.*

McCarthy, J. and Zachara, J., 1989. Subsurface transport of contaminants, *Environ. Sci. Technol.* **23/5**, pp 496-502.

McDonald, R., Isbell, R., Speignt, J., Walker, J. and Hopkins, M., 1984. Australian soil and land survey field handbood, Inkata Press, Melbourne.

McSweeny, K. and Madison, F., 1988. Formation of a cemented subsurface horizon in sulfide minewaste, *J. Environ. Qual*, **17/2**, pp 258-261.

Mermut, A., Curtin, D. and Rostad, H., 1985. Micromorphological and submicroscopical features related to pyrite oxidation in an inland marine shale from east central Saskatchewan, *Soil Sci. Soc. Am. J.*, **49**.

Miller, S., Jeffery, J. and Donohue, T., 1994. Developments in predicting and management of acid forming mine wastes in Aust. and Southeast Asia, *in* International land reclamation and mine drainage conference and the third international conference on the abatement of acidic drainage, Pittsburgh, PA, April 24-29, **1**, pp 177-184.

Milnes, A., Wright, M. and Thiry, M., 1991. Silica Accumulations in saprolites and soils in SA., *Occurrence, Characteristics and Genesis of Carbonate, Gypsum and silica Accumulations in soils.* SSSA special pub **26**, pp 121-149. Soil Sci. Soc. of Am.

Milnes, A., 1991. (CSIRO) Personal communication with Mr R. Wildy (SADME) chairman of the Brukunga site Management Steering committee.

Mirams, R., 1963. Report on pyrite-pyrrhotite deposit of Nairne, *SADME report* **56/83. G.S 2591, D.M 646/63**.

Modak, D., Singh, K., Chandra, H. and Ray, R. 1992. Mobile and Bound forms of trace metals in sediments of the lower Ganges, *Wat. Res.* **26/11**, pp 1541-1548.

Morin, K., 1988. Physical and chemical hydrogeology of uranium tailings in Canada and the United States of America, Proceedings Internat. Groundwater Symp., Internat. Assoc, Hydrogeologists, Halifax, Nova Scotia.

Morin, K. and Cherry, J,. 1988. Migration of acid groundwater seepage from uranium tailings impoundments, 3. Simulation of the conceptual model with application to seepage area, A. *J. Contam. Hydrology* **2**.

Morin, K., Cherry, J., Dave, N., Lim, T., and Vivyurka, A., 1988a. Migration of acidic groundwater seepage from uranium-tailings impoundments, 1. Field study and conceptual hydrogeochemical model, *J. Contam. Hydrology* **2**.

Morin, K., Cherry, J., Dave, N., Lim, T., and Vivyurka, A., 1988b. Migration of acidic groundwater seepage from uranium-tailings impoundments, 2. Behaviour of radionuclides in water, *J. Contam. Hydrology* **2**.

Morse, J., Millero, F., Cornwell, J. and Rickard, D., 1987. The chemistry of the hydrogen sulfide and iron sulfide systems in Natural waters, *Earth Science Reviews* **24**, pp 1-42.

Mustin, C., Berthelin, J., Marion, P. and DeDonato, P., 1992. Corrosion and electrochemical oxidation of a pyrite by *Thiobacillus ferrooxidans*, *Applied Environ. Microbiology*, **58/.4**, pp 1175-1182.

Newcrest Mining Ltd, 1992. Tailings management course and seminar, April 14-16, Belmont Office, 179 Great Eastern Highway.

Nordstom, D., 1982. Aqueous Pyrite oxidation and the consequent formation of secondary iron minerals *in* Kittrick, J., Fanning, D. and Hossner, L., 1987. Acid sulfate weathering, Soil Sci. Soc. of Am., Wisconsin, pp 37-62.

O'shay, T., Hossner, L. and Dixon, J., 1990. A modified hydrogen peroxide oxidation method for determination of potential acidity in pyritic overburden, *J Environ. Qual*, **19**.

Palache, C., Berman, H. and Frondel, C., 1951. Dana's system of mineralogy, John Wiley and Sons, Inc.

Patrick, W. and Mahapatra, I. 1968. Transformations and availability of nitrogen and phosphous in water-logged soils, *Advan. Agron.*, **20**. sited in Bohn, H., 1971. Redox Potentials. *Soil Sci.*, **112**.

Pons, L., van Breemen, N. and Dressen, P., 1982. Physiography of coastal sediments and development of potential soil acidity. *in* Kittrick, J., Fanning, D. and Hossner, L., (Eds) Acid sulfate weathering Soil Sci. Soc. Am., spec Pub. **10**. Soil Sci. Soc. Am., Madison Wisconsin

Postgate, J., 1979. The sulfate -reducing bacteria, Cambridge University Press.

Pugh, C., Hossner, L. and Dixon, J., 1984. Oxidation rate of iron sulfides as affected by surface area, morphology, oxygen conc, and autotrophic bacteria, *Soil Sci.* **137/5**, pp 309-314.

Pugh, C., Hossner, L. and Dixon, J., 1981. Pyrite and marcasite surface area as influenced by morphology and particle diameter, *Soil Sci. Soc. Am. J.*, **45**, pp 978-982.

Rabenhorst, M. and James, B., 1992. Iron sulfidisation in tidal marsh soils *in* Skinner, H. and Fitzpatrick, R., (Eds) Biomineralisation - Processes of iron and manganese. Catena Verlag, Germany.

Rayment, G. and Higgenson, F., 1992. Australian laboratory handbook of soil and water chemical methods, Inkata Press, Sydney, Aust.

Read, R., 1986. Brukunga Mine, Investigations of Acid drainage, Geological Survey. *SADME report*, **86/83**.

Reclamation Research Unit, 1987. Acid forming materials Symposium, *Reclamation Research Pub*.

Ridgeway, J., 1949. Gibralta Pyrite mine, *SADME report*, pp 80-91.

Rickard, D., 1973. Sedimentary iron sulfide formation *in* Acid sulfate soils International Land Reclamation Institute, Pub **18**, Wageningen, Netherlands.

Ritchie, G., 1989. Tailings Management-Problems and solutions in the mining industry, Elsevier Sci. Pub. Co.

Ross.G., Wang, C., Ozkan, A. and Rees, H., 1982. Weathering of chlorite and mica in a new Brunswick podzol developed on till derived from chlorite-mica schist, *Geoderma* **27**.

Schueck, J., 1988. Mapping Buried Tripple Refuse - is the magnetometer better than terrain conductivity, Mine drainage and surface main reclamation, Proc. Conf. Pittsburgh, pp 117-130.

Schwarcz, H. and Burnie, S., 1973. Influence of sedimentary environmnents on sulfur isotope ratios in clastic rocks: a review, *Miner. Deposita*, **8**, pp 264-277.

Schwertmann, U. and Thalmann, H. 1976. The influence of Fe(II), Si and pH on the formation of lepidocrocite and ferrihydrite during oxidation of aqueous $FeCl_2$ solutions, *Clay minerals*, **11/189**, pp 189-199.

Scott, K., 1987. Solid solution in, and classification of, gossan-derived members of the alunite-jarosite family, north west Qld, Aust., *American Mineralogist*, **73**, pp 178-187.

Seccombe, P., Spry, P., Both, R., Jones, M. and Schiller, J., 1985. Base metal mineralisation in the Kanmantoo Group, SA: a regional sulfur isotope study, *Economic Geology*, **80**, pp 1824-1841.

Sendlein, L., Yazicigil, H. and Carlson, C., 1983. Surface mining environmental monitoring and reclamation handbook, Elsevier Sci. Pub. Co. Inc.

Sengupta, M., 1993. Environmental Impacts of mining, monitoring, restoration and control, Lewis Pub.

Singer, P. and Stumm, W., 1970. Acidic mine drainage: the rate determining step, *Science*, pp 112-1123.

Skinner, B., 1958. The geology and metamorphism of the Nairne pyritic formations, a sedimentary sulfide deposit in SA., *Economic Geology* **53**, pp 546-562.

Skinner, H. and Fitzpatrick, R., (Eds), 1992. Biomineralisation - Processes of iron and manganese, Catena Verlag, Germany.

Smith, A.D., 1955. Notes on treatment plant at Nairne pyrite Ltd., *SADME, report* **41/76**.

Smith, P. and Hancock, S., 1992. Brukunga - the acid test, *Waste disposal and water management in Australia*, Dec 1992.

Soil Survey Staff, 1992. Keys to soil taxonomy 5th Ed., *Soil Management support services*. Technical monograph **19**. Pocahonts Press Inc.

S.A. Housing Trust, 1992. Brukunga - Investigations for health risk assessment of SAHT Housing for soils, leachates and crystalline deposits, *SAHT report*.

SADME, 1989. Brukunga mine rehabilitation conceptual plan - April, *JN Report* **5059A**.

SADME, 1987. Rehabilitation of the Brukunga pyrites mine - status report, *SADME report*.

Sullivan, P., Yelton, J. and Reddy, K., 1988. Iron sulfide oxidation and the chemistry of acid generation, *Environ. Geol. Water Sci.* **11/3**, pp 289-295. Springer-Verlag New York Inc.

Talsma, T. and Philip, J. (Eds) 1971. Salinity and Water Use, Macmillan Press.

Taylor, G., Oxidation and supergene enrichment of massive sulfide deposits, Unpub report.

Taylor, G. and Appleyard, E., 1983. Weathering of the zinc - lead lode, Dugald River, north-west Qld: I The gossan profile, *J. of Geochemical exploration*, **18**, pp 87-110.

Taylor, G. and Scott, K., 1983. Weathering of the zinc - lead lode, Dugald River, north-west Qld: II Surface mineralogy and geochemistry, *J. of Geochemical exploration*, **18**, pp 111-130.

Taylor, G. and Sylvester, G., 1982. Analysis of a weathered profile on sulfide mineralisation at Mugga Mugga, WA., *AA*, **16**, pp 105-134.

Taylor, R. and Hardy, R., 1973. Sulfate species in colliery spoil banks, *Trans. Inst. Mining and Metall.* Section A, **83**, pp 123-126.

Thiry, M. and Milnes, A., 1991. Pedogenic and groundwater silcretes at Stuart Creek opal field, SA., *J. of Sedimentology Petrology*, **61/1**, pp 11-123.

Toteff, S., 1977. The geology of the Adelaidean - Kanmantoo Group sequences in the eastern Mount Lofty Rangers, B.Sc (Hons) University of Adelaide.

Vepraskas, M., 1992. Redoximorphic features for identifying aquic conditions, *North Carolina Ag. Research Service*. Technical Bulletin **301**.

Walker, W., 1977a. Rehabilitation of Brukunga pyrite mine, *Amdel report* **1149**.

Walker, W., 1977a. Rehabilitation of Brukunga pyrite mine- Mullock heap revegetation, *Amdel report*, **1170**.

Walker, W., 1986. Rehabilitation of Brukunga pyrite mine- 1985/86 progress report, *Amdel report*, **1/1/145**.

Wiggering, H., 1987. Weathering of clay minerals in waste dumps of upper carboniferous coal-bearing strata, the Ruhr Area, West Germany, *Applied Clay Sci.*, **2**, pp 353-361.

Williams, B. and Pannewig, M., 1994. A reconnaissance electromagnetic inducation survey of the Brukunga pyrites mine tailings dump, Unpub.

Winland, R., Traina, S. and Bigham, J., 1991. Chemical composition of ochreous precipitates from Ohio Coal mines drainage, *Environ. Qual.*, **20**, pp 452-460.

Yanful, E. and St Arnaud, L., 1991. The Waite Amulet hydrogeochemical evolution, Proc. 2nd Int. Conf. on the Abatement of acidic drainage, Montreal, Mend CANMET, pp 91-114.

Yaron, B., Dagan, G. and Goldshmid, J., 1984. Pollutants in porous media *in* Ecological studies **47**.

Yong, R., Mohamed, A. and Warkentin, B., 1992. Principles of contaminant transport in soils, Elsevier Sci. Pub. Co.